ELSEVIER

Marine Micropaleontology 38 (2000) 181–211

MARINE MICROPALEONTOLOGY

www.elsevier.com/locate/marmicro

Integrated stratigraphy and astronomical calibration of the Serravallian/Tortonian boundary section at Monte Gibliscemi (Sicily, Italy)

F.J. Hilgen [a,*], W. Krijgsman [b], I. Raffi [c], E. Turco [a], W.J. Zachariasse [a]

[a] *Department of Geology, Utrecht University, Budapestlaan 4, 3584 CD Utrecht, The Netherlands*
[b] *Paleomagnetic Laboratory, Fort Hoofddijk, Budapestlaan 17, 3584 CD Utrecht, The Netherlands*
[c] *Dip. di Scienze della Terra, Univ. G. D'Annunzio, via dei Vestini 31, 66013 Chieti Scalo, Italy*

Received 12 May 1999; revised version received 20 December 1999; accepted 26 December 1999

Abstract

Results are presented of an integrated stratigraphic (calcareous plankton biostratigraphy, cyclostratigraphy and magnetostratigraphy) study of the Serravallian/Tortonian (S/T) boundary section of Monte Gibliscemi (Sicily, Italy). Astronomical calibration of the sedimentary cycles provides absolute ages for calcareous plankton bio-events in the interval between 9.8 and 12.1 Ma. The first occurrence (FO) of *Neogloboquadrina acostaensis*, usually taken to delimit the S/T boundary, is dated astronomically at 11.781 Ma, pre-dating the migratory arrival of the species at low latitudes in the Atlantic by almost 2 million years. In contrast to delayed low-latitude arrival of *N. acostaensis*, *Paragloborotalia mayeri* shows a delayed low-latitude extinction of slightly more than 0.7 million years with respect to the Mediterranean (last occurrence (LO) at 10.49 Ma at Ceara Rise; LO at 11.205 Ma in the Mediterranean). The *Discoaster hamatus* FO, dated at 10.150 Ma, is clearly delayed with respect to the open ocean. The ages of *D. kugleri* first and last common occurrence (FCO and LCO), *Catinaster coalitus* FO, *Coccolithus miopelagicus* last (regular) occurrence (L(R)O) and the *D. hamatus*/*neohamatus* cross-over, however, are in good to excellent agreement with astronomically tuned ages for the same events at Ceara Rise (tropical Atlantic), suggesting that both independently established timescales are consistent with one another. The lack of a reliable magnetostratigraphy hampers a direct comparison with the geomagnetic polarity timescale of Cande and Kent (1995; CK95), but ages of calcareous nannofossil events suggests that CK95 is significantly younger over the studied time interval. Approximate astronomical ages for the polarity reversals were obtained by exporting astronomical ages of selected nannofossil events from Ceara Rise (and the Mediterranean) to eastern equatorial Pacific ODP Leg 138 Site 845, which has a reliable magnetostratigraphy.

Our data from the Rio Mazzapiedi–Castellania section reveal that the base of the Tortonian stratotype corresponds almost exactly with the first regular occurrence (FRO) of *N. acostaensis* s.s. as defined in the present study, dated at 10.554 Ma. An extrapolated age of 11.8 Ma calculated for the top of the Serravallian stratotype indicates that there is a gap between the top of the Serravallian and the base of the Tortonian stratotype, potentially rendering all bio-events in the interval between 11.8 and 10.554 Ma suitable for delimiting the S/T boundary. Despite the tectonic deformation and the lack of a magnetostratigraphy, Gibliscemi remains a candidate to define the S/T boundary by means of the Tortonian global boundary stratotype section and point (GSSP). © 2000 Elsevier Science B.V. All rights reserved.

* Corresponding author. E-mail: fhilgen@geo.uu.nl

0377-8398/00/$ – see front matter © 2000 Elsevier Science B.V. All rights reserved.
PII: S0377-8398(00)00008-6

Keywords: Serravallian/Tortonian boundary; calcareous plankton biostratigraphy; cyclostratigraphy; astronomical timescale; Mediterranean Neogene

1. Introduction

Stability in both chronostratigraphic standards and chronometric timescales is needed to facilitate communication between earth scientists. Stability in chronostratigraphic standards can be achieved by carefully selecting global boundary stratotype sections and points (GSSPs) following the procedures and guidelines set by the International Commission on Stratigraphy (ICS; Remane et al., 1996). Stability in chronometric timescales is less easily achieved and depends, among others, on caution not to publish new timescales on a too frequent basis (see also Berggren et al., 1995). Such a stability is now within reach for the youngest part of the Earth's history because astronomical timescales attain a permanent character and need to undergo no or only minor revisions in the future (e.g., Langereis et al., 1994; Lourens et al., 1996), thus avoiding the promulgation of new and fundamentally different timescales. For the Plio–Pleistocene, the astronomical timescale is now well established and accepted as a standard (Cande and Kent, 1995; Berggren et al., 1995). An additional advantage is that (proposed) chronostratigraphic boundaries such as the GSSPs for the Pliocene stages and the Pliocene/Pleistocene boundary are directly tied to the astronomical timescale via first-order correlations in the Mediterranean.

Recently, the astronomical timescale has been extended into the Miocene (Hilgen et al., 1995; Shackleton and Crowhurst, 1997) and includes the Tortonian/Messinian boundary. In the Mediterranean, the (Late) Miocene extension — back to 9.8 Ma — was based primarily on two long(er) sections, the Metochia section on Gavdos and the Gibliscemi section on Sicily. On Gavdos, further extension to older levels is not possible due to the presence of a hiatus. This hiatus is associated with shallow marine sandstones and estuarine-type sediments which directly underlie the astronomically dated, open marine sediments of the Tortonian (see Postma et al., 1993). At Gibliscemi, however, older cyclically bedded sediments are exposed about 1 km southeast of the previously studied section. Despite the intense deformation, we were able to log and sample a continuous succession which covers the interval between 9.8 and 12.1 Ma. This interval contains the Serravallian/Tortonian (i.e., Middle/Upper Miocene) boundary, commonly placed at or close to the first occurrence of *Neogloboquadrina acostaensis* in the Mediterranean (Rio et al., 1997).

This paper presents the cyclostratigraphy, magnetostratigraphy, and calcareous plankton biostratigraphy of the Serravallian/Tortonian boundary section at Monte Gibliscemi. Sedimentary cycles are correlated to astronomical target curves. The resultant — astronomically dated — biochronology is compared, among others, with that of similarly dated Ocean Drilling Project (ODP) sequences and implications for the Serravallian/Tortonian boundary are discussed.

2. Geological setting and location

The Gibliscemi section is named after Monte Gibliscemi on Sicily and is located 10 km southwest of section Giammoia (Fig. 1). Both sections contain a deep-marine cyclically bedded hemipelagic succession of Miocene age which overlie intensely deformed multi-coloured clays of the 'Argille Scagliose'. The succession starts with an alternation of homogeneous marls and sapropels, followed by diatomites of the Tripoli Formation, and capped by Calcare di Base limestones of the Gessoso–Solfifera Formation. The latter represent the sedimentary expression of the Messinian salinity crisis in the Mediterranean.

The entire succession was deposited in the Caltanissetta Basin which became part of the Apenninic–Maghrebian foredeep that developed externally to the evolving orogen. The succession was incorporated into the African-verging thrust wedge during the Plio–Pleistocene, the 'Argille Scagliose'

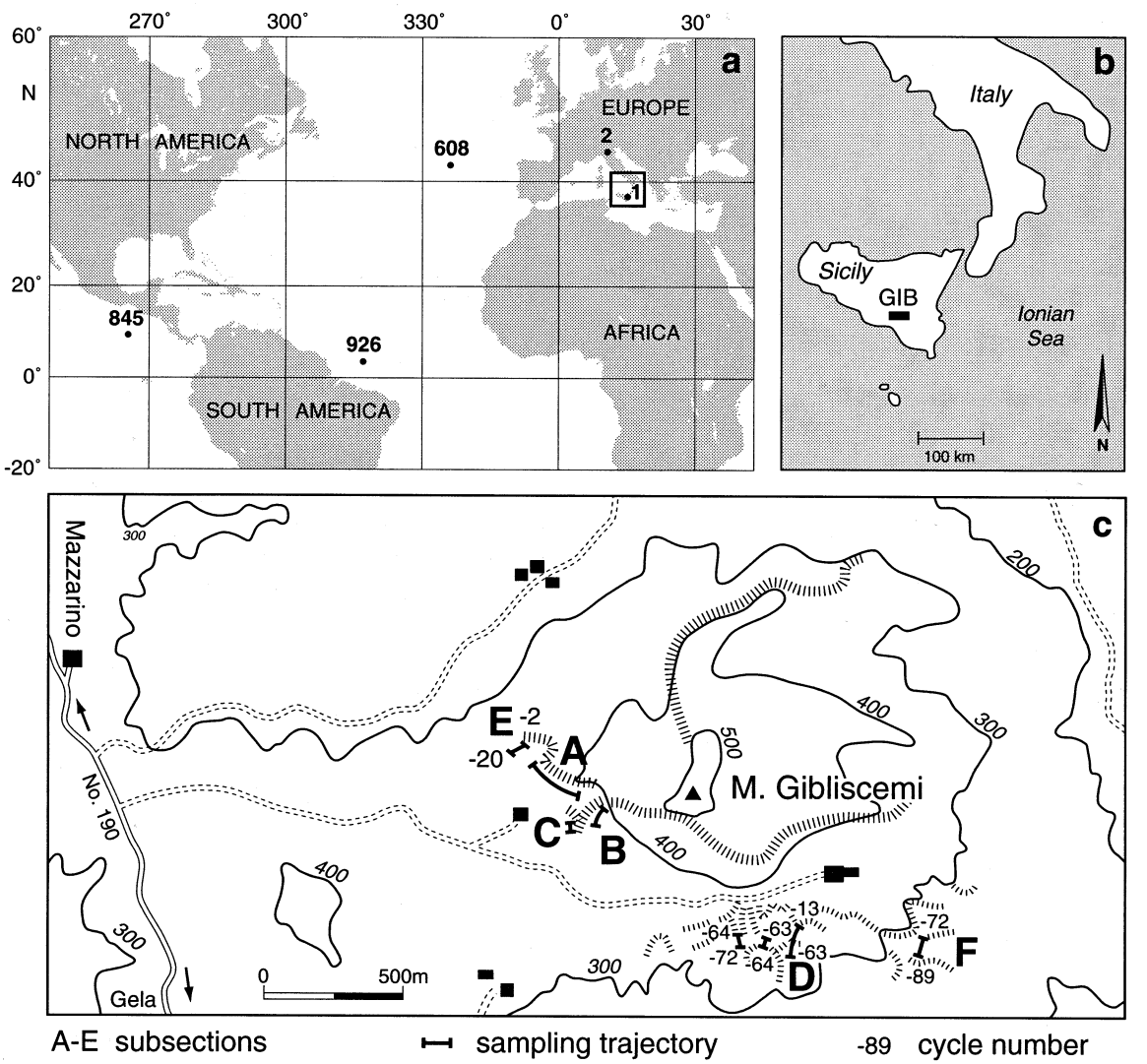

Fig. 1. Location maps of the sections and DSDP/ODP sites mentioned in the text (a) and of the studied (sub)sections at Monte Gibliscemi (b, c). Subsections *C* and *E* are located in the western gully complex, subsections *D* and *F* in the southern complex.

acting as a lubricant for decollement. The African foreland is represented by the nearby Ragusa platform of southeastern Sicily (see Fig. 1). Despite the close proximity to the foreland, deformation in the Gibliscemi sections is extensional only and, especially in the lower parts, consists of low-angle shear planes which tectonically reduce the stratigraphy.

3. Sections and lithology

The pre-evaporite part of the sedimentary succession is well-exposed in the two main gully complexes along the southern slopes of Monte Gibliscemi. The western complex accommodates the Gibliscemi A/B composite and Gibliscemi C and E. Gibliscemi D and F are located in the southern complex (see Fig. 1). The present study focuses entirely on the Gibliscemi C/D/E/F composite.

Most of the sedimentary cycles in Gibliscemi C/D/E/F consist of a whitish-coloured homogeneous marl and a dark, grey-coloured marl (or marly clay). The darker-coloured marls are replaced by brownish, often laminated beds termed sapropels in the top and bottom part of the section so that the cycles become identical to those in the previously studied Gibliscemi A/B section (Krijgsman et al., 1995; Hilgen et al., 1995). Close inspection reveals that the cycles are not strictly bipartite but quadripartite due to the intercalation of a greyish beige marl within the light-coloured homogeneous marl. In this respect, the cycles bear a resemblance to the quadripartite carbonate cycles of the Pliocene Trubi Formation on Sicily (Hilgen, 1987). Reddish-coloured bands are occasionally present either as distinct thin bands above the darker grey marls or as more diffuse and thicker bands below them and may reflect paleoredox fronts along which iron-oxides precipitated during early diagenesis. Four distinct fine-grained ash layers are found in the lower part of the section.

Individual sedimentary cycles in the C/D/E/F composite were labelled 'G 0' to 'G −89' because cycles in Gibliscemi A/B have previously been numbered G1 to G85 (Krijgsman et al., 1995). The (negative) numbering has been maintained here to avoid confusion arising from renumbering cycles in the entire Gibliscemi composite. Because of the deformation, no continuous succession could be logged and sampled along a single trajectory or in a single subsection. Gibliscemi D is a composite section itself and consists of various subsections located throughout the southern gully complex (see Figs. 1 and 2). Stratigraphic correlations between subsections are based on identification of the characteristic sedimentary cycle pattern.

The construction of a reliable composite was not an easy task due to the locally intense deformation. In particular, the cyclostratigraphy of the upper part

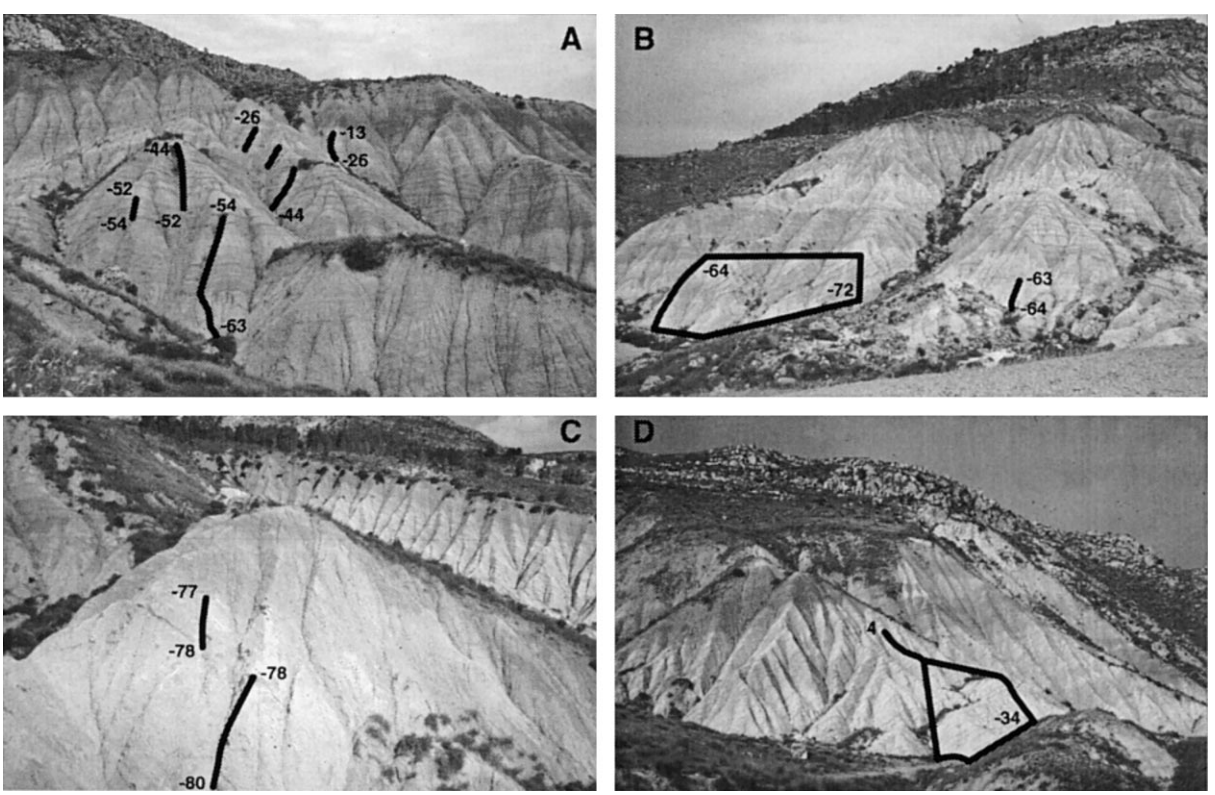

Fig. 2. Photographs of subsections Gibliscemi D (A, B) and Gibliscemi F (C), and of section Giammoia (D), showing (part of the) sample trajectory and numbered sedimentary cycles.

of Gibliscemi D and the stratigraphic link between Gibliscemi A/B and C/D/E were difficult to ascertain. The A/B and C/D/E sections were linked using the approximate number of cycles in the deformed interval between 0 and −11 in combination with the prominent character of (the sapropel of) cycle −4. The upper part of Gibliscemi D includes 5 cycles (−23 to −28) that are only present in the gully sampled (Fig. 2A). These cycles are partly missing (i.e., via tectonic reduction) in the next gully (used for sampling cycles −26 to −44) and are not found again in the entire Gibliscemi D gully complex. Both the presence of the 5 extra cycles as well as the exact number of cycles between 0 and −11 were confirmed at Monte Giammoia, in a section located 100 m west of the main gully of section Giammoia 3 (de Visser, 1991; see Fig. 2B). Despite the apparent deformation, the interval from cycle −33 to 4 could be logged in this section; a shear plane truncates the top of (the characteristic) cycle 4 with its distinctly yellow-colour band.

The lowermost part of Gibliscemi D is strongly deformed and the cycle pattern is less certain. This interval was logged and sampled in Gibliscemi F, located several hundreds of metres east of Gibliscemi D (Figs. 1 and 2D). For the lowermost part (cycle −84 to −89), the succession is again confirmed at Gibliscemi D.

4. Astronomical calibration and age model

Sedimentary cycles are not distributed evenly throughout the succession but reveal distinct patterns. These patterns allow to distinguish both small-scale as well as large-scale clusters of the basic sedimentary cycle. Small-scale clusters usually contain 2 to 4 basic cycles whereas larger-scale clusters may contain several small-scale clusters. This subdivision is particularly evident in the lower half of the section but — although less obvious — can also be recognised in the upper part on the basis of the occurrence of aberrantly thick homogeneous marl beds and/or variations in the distinctness of the grey marl beds.

The observed cycle patterns — with clusters on different scales superimposed on the basic sedimentary cycle — are identical to those observed in the Mediterranean Late Miocene and Pliocene–Pleistocene (Hilgen, 1991; Hilgen et al., 1995; Lourens et al., 1996). Using oxygen isotope stratigraphy, a sapropel chronology was established for the last 0.5 million years (Hilgen, 1991). This chronology was compared with computed astronomical curves for the past variations in the Earth's orbit and spin-axis to determine phase relations between the sapropel cycles and the astronomical cycles: individual sapropels correspond to precession minima/summer insolation maxima, and small-scale and large-scale sapropel clusters to 100,000 and 400,000 years eccentricity maxima (Hilgen, 1991), while alternating thin–thick sapropels reflect precession/obliquity interference (Lourens et al., 1996). Further research showed that the sapropels are the equivalent of grey-coloured $CaCO_3$-poor marl beds in the basic carbonate cycles of the Pliocene Trubi Formation of southern Italy while a multidisciplinary study of three 9.5-Ma-old sapropels revealed that the basic mechanism of cycle formation remained essentially the same over the last 10 million years (Schenau et al., 1999). Pliocene–Pleistocene phase relations between sedimentary and orbital cycles can therefore be applied to astronomically calibrate (older) sedimentary cycles like those in the Gibliscemi sections (Hilgen et al., 1995). For this purpose, we used the $La90_{(1,1)}$ solution (Laskar, 1990; Laskar et al., 1993) with present-day values for the dynamical ellipticity of the Earth and the tidal dissipation by the moon, because this solution was previously shown to be in perfect agreement with all the intricate details of sedimentary cycle patterns in the Mediterranean Pliocene–Pleistocene, including precession/obliquity interference as reflected in the 65° northern-latitude summer-insolation target curve (Lourens et al., 1996).

Sedimentary cycles in the Gibliscemi A/B composite were tuned using a stepwise approach (Hilgen et al., 1995). Firstly, the magnetostratigraphy of (parallel) sections, that were correlated cyclostratigraphically in detail to Gibliscemi A/B, was calibrated to the polarity timescales of Cande and Kent (1995; CK95) and Shackleton et al. (1995; SCHPS95). Secondly, the ages of CK95 and SCHPS95 for the polarity reversals and especially for the youngest polarity reversal recorded in our sections were taken as starting point for the actual tuning. Thirdly, the additional use of Pliocene–Pleistocene phase rela-

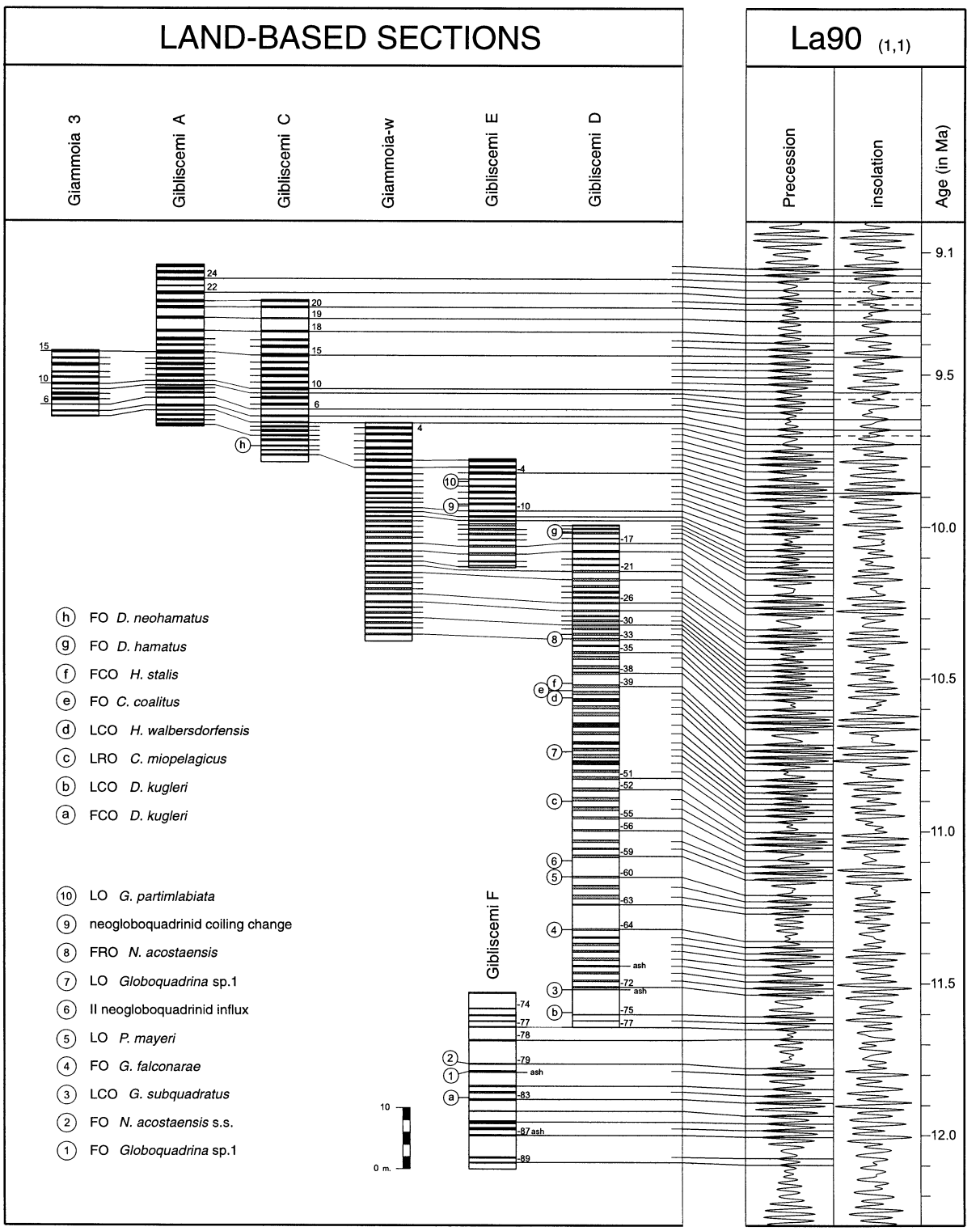
LAND-BASED SECTIONS
La90 (1,1)
Giammoia 3
Gibliscemi A
Gibliscemi C
Giammoia-w
Gibliscemi E
Gibliscemi D
Gibliscemi F
Precession
insolation
Age (in Ma)
9.1
9.5
10.0
10.5
11.0
11.5
12.0
h FO D. neohamatus
g FO D. hamatus
f FCO H. stalis
e FO C. coalitus
d LCO H. walbersdorfensis
c LRO C. miopelagicus
b LCO D. kugleri
a FCO D. kugleri
10 LO G. partimlabiata
9 neogloboquadrinid coiling change
8 FRO N. acostaensis
7 LO Globoquadrina sp.1
6 II neogloboquadrinid influx
5 LO P. mayeri
4 FO G. falconarae
3 LCO G. subquadratus
2 FO N. acostaensis s.s.
1 FO Globoquadrina sp.1
10
0 m.
ash

tions between astronomical and sedimentary cycles allowed to establish a — first-order — tuning by correlating firstly large-scale sapropel clusters to 400,000-year eccentricity maxima followed by the correlation of small-scale clusters to 100,000-year maxima. This resulted in an adjustment of the initial age estimates of the polarity reversals. Fourthly, the astronomical calibration of the Gibliscemi A/B composite was completed by tuning individual sapropels to precession minima and the corresponding summer insolation maxima. The tuning resulted in a good to excellent fit between characteristic patterns in the astronomical and sedimentary cycle records, including precession/obliquity interference back to 9.5 Ma (Hilgen et al., 1995).

Starting from the astronomical tuning of the younger sedimentary cycles in section Gibliscemi A/B, we calibrated successively older cycles in the Gibliscemi C/D/E/F composite to the astronomical record, using a pattern-matching procedure similar to that described by Hilgen et al. (1995). During the tuning exercise, larger-scale eccentricity-related cycle patterns were taken into account, because they provide a direct check on the validity of the calibration and prevent errors in the tuning of the individual cycles to accumulate. This approach resulted in the astronomical calibration of the sedimentary cycles presented in Fig. 3. The tuning is probably accurate to the level of the individual precession/insolation cycle in certain intervals but may be off by one cycle in others. For instance, details in the sedimentary cycle pattern indicate that cycles −10 to −17 better correspond to one insolation maximum older. But in that case, one sedimentary cycle should have been eliminated by tectonic reduction for which we have no evidence. At this stage it is not clear whether such misfits arise from minor stratigraphic discontinuities or from small inadequacies in the astronomical solution. The calibration provides absolute astronomical ages both for the sedimentary cycles (Table 1) as well as for the recorded bio-events (Table 2).

5. Biostratigraphy and biochronology

5.1. Planktonic foraminifera

Fig. 4 shows the quantitative distribution pattern of 10 planktonic foraminiferal categories having biostratigraphic significance. These patterns are based on counting all planktonic foraminifers from splits of the >125-μm fraction in 502 samples. A full report of all census data is given as a background data set (http://www.elsevier.nl/locate/marmicro; mirrorsite: http://www.elsevier.com/locate/marmicro) to this paper. A qualitative analysis based on surveying a standard number of fields (27 out of 45) on a rectangular picking tray, containing between 30,000 and 40,000 specimens, of samples positioned around the observed bio-events showed that the actual position of a limited number of biohorizons (as presented in Fig. 4 and Table 2) is maximally 4 samples off from their position based on the quantitative analysis only. Preservation is generally good, and on average slightly better in the sapropels than in the homogeneous intervals where specimens are often filled and sometimes even recrystallised. Taxonomy and distribution patterns of the biostratigraphic marker species are discussed in more detail in the next paragraphs.

5.1.1. Globoquadrina sp. 1 and Globorotaloides falconarae

Globoquadrina sp. 1 differs from *Globoquadrina dehiscens* by a smaller average test-size, looser coiling, less flattened apertural face, less pronounced tooth plates and a more convex spiral side (Plate 1, 1–7). This species is most likely an immigrant and seems to have evolved into *Globorotaloides falconarae* (Plate 1, 8–12). The latter species has been described by Giannelli and Salvatorini (1976) from the Mediterranean, but considered by Zachariasse (1992) to be a junior synonym of *Catapsydrax parvulus* described by Bolli (1957) from Trinidad (Plate 1, 13–15). The small-sized type of *G. falconarae*, which in

Fig. 3. Astronomical tuning of the sedimentary cycles in the downward extension of the Gibliscemi section and position of the main calcareous plankton events. Black layers denote sapropels and hatched/shaded layers grey marl beds intercalated in light(er)-coloured homogeneous marls (indicated as white layers). Darker and lighter shading schematically indicate differences in the grey scale of the grey marl beds. Numbers to the right of the lithological columns denote cycle numbers. Horizontal lines show selected (characteristic) cycles and their preferred astronomical calibration. $La90_{(1,1)}$ refers to the astronomical solution of Laskar (1990) and Laskar et al. (1993) with present-day values for tidal dissipation and the dynamical ellipticity of the Earth.

Table 1
Stratigraphic position and astronomical ages of the sedimentary cycles 1 down to −89 in the Gibliscemi C/D/E/F composite section

Grey/sap.	Bottom–top (m)	Mid-point	Age (ka)	Grey/sap.	Bottom–top (m)	Mid-point	Age (ka)
Cycle 1	114.99–115.12	115.055	9,773	Cycle −44	70.02–70.67	70.345	10,832
Cycle 0	114.13–114.43	114.280	9,795	Cycle −45	68.82–69.27	69.045	10,852
Cycle −1	113.26–113.47	113.365	9,817	Cycle −46	67.32–67.82	67.570	10,873
Cycle −2	112.55–112.75	112.650	9,843	Cycle −47	66.27–66.62	66.445	10,892
Cycle −3	111.56–111.92	111.740	9,866	Cycle −48	65.17–65.67	65.420	10,910
Cycle −4	110.59–110.98	110.785	9,888	Cycle −49	64.07–64.67	64.370	10,928
Cycle −5	109.70–109.88	109.790	9,909	Cycle −50	62.87–63.22	63.045	10,948
Cycle −6	108.57–108.85	108.710	9,932	Cycle −51	61.77–62.17	61.970	10,968
Cycle −7	107.58–107.92	107.750	9,959	Cycle −52	59.92–60.37	60.145	11,002
Cycle −8	106.68–106.85	106.765	9,980	Cycle −53	58.37–58.87	58.620	11,023
Cycle −9	105.73–106.00	105.865	10,002	Cycle −54	56.82–57.42	57.120	11,043
Cycle −10	104.62–104.88	104.750	10,023	Cycle −55	55.52–55.82	55.670	11,064
Cycle −11	103.71–103.99	103.850	10,057	Cycle −56	53.57–53.92	53.745	11,093
Cycle −12	103.10–103.27	103.185	10,076	Cycle −57	51.77–52.17	51.970	11,116
Cycle −13	102.37–102.71	102.540	10,095	Cycle −58	50.67–50.97	50.820	11,137
Cycle −14	101.69–101.97	101.830	10,114	Cycle −59	49.37–49.77	49.570	11,158
Cycle −15	100.91–101.19	101.050	10,132	Cycle −60	46.15–46.40	46.275	11,209
Cycle −16	99.97–100.22	100.095	10,152	Cycle −61	44.40–44.95	44.675	11,230
Cycle −17	98.97–99.30	99.135	10,172	Cycle −62	42.80–43.40	43.100	11,251
Cycle −18	97.71–98.07	97.890	10,223	Cycle −63	41.80–41.95	41.875	11,270
Cycle −19	96.61–96.85	96.730	10,244	Cycle −64	37.80–38.05	37.925	11,361
Cycle −20	95.71–96.08	95.895	10,266	Cycle −65	36.55–36.80	36.675	11,380
Cycle −21	94.66–94.96	94.810	10,287	Cycle −66	35.40–35.75	35.575	11,401
Cycle −22	93.31–93.66	93.485	10,308	Cycle −67	34.35–34.60	34.475	11,422
Cycle −23	92.26–92.61	92.435	10,338	Cycle −68	33.05–33.45	33.250	11,443
Cycle −24	91.36–91.66	91.510	10,359	Cycle −69	32.00–32.25	32.125	11,471
Cycle −25	90.51–90.76	90.635	10,379	Cycle −70	30.95–31.20	31.075	11,493
Cycle −26	89.66–89.91	89.785	10,400	Cycle −71	29.70–29.95	29.825	11,515
Cycle −27	88.41–88.66	88.535	10,435	Cycle −72	28.70–28.90	28.800	11,536
Cycle −28	87.59–87.79	87.690	10,453	Cycle −75	24.63–24.71	24.670	11,608
Cycle −29	86.79–87.09	86.940	10,473	Cycle −76	23.65–23.71	23.680	11,629
Cycle −30	86.14–86.39	86.265	10,492	Cycle −77	22.61–22.65	22.630	11,650
Cycle −31	85.49–85.79	85.640	10,511	Cycle −78	20.56–20.69	20.625	11,683
Cycle −32	84.64–84.94	84.790	10,530	Cycle −79	16.73–16.88	16.805	11,778
Cycle −33	83.79–84.14	83.965	10,550	Cycle −80	15.63–15.73	15.680	11,799
Cycle −34	82.84–83.04	82.940	10,570	Cycle −81	13.18–13.43	13.305	11,846
Cycle −35	81.74–82.04	81.890	10,602	Cycle −82	12.16–12.41	12.280	11,870
Cycle −36	80.79–81.29	81.040	10,623	Cycle −83	10.98–11.28	11.130	11,892
Cycle −37	79.34–79.79	79.565	10,644	Cycle −84	9.23–9.33	9.280	11,936
Cycle −38	78.39– 78.74	78.565	10,665	Cycle −85	7.22–7.73	7.475	11,961
Cycle −39	76.28– 76.74	76.510	10,716	Cycle −86	6.27–6.66	6.465	11,984
Cycle −40	75.19– 75.67	75.430	10,737	Cycle −87	5.28–5.51	5.395	12,006
Cycle −41	74.07– 74.57	74.320	10,759	Cycle −88	1.78–1.98	1.880	12,077
Cycle −42	72.94– 73.39	73.165	10,779	Cycle −89	0.95–1.08	1.015	12,098

Ages refer to the mid-point of grey layers and/or sapropels and represent non-lagged ages of the correlative precession minimum.

the Mediterranean prevailed between 8.87 and 7.46 Ma (Hilgen et al., 1995) is indeed virtually indistinguishable from *C. parvulus*. The present study, however, suggests that *G. falconarae* evolved from *Globoquadrina* sp. 1 in post-Zone N14 levels, whereas the range of the low-latitude *C. parvulus* extends back into the Early Miocene where it might root in the group of *Catapsydrax* (Kennett and Srinivasan, 1983). All

Table 2
Stratigraphic position and astronomical ages of calcareous plankton events

Species	Event	Cycle	Position	Age
Planktonic foraminifer:				
Globorotalia partimlabiata	LO	−5/−6	109.45–109.73	9.913 ± 0.003
Neogloboquadrina group	d/s	−10	105.30–105.46	10.011 ± 0.002
Neogloboquadrina acostaensis s.s.	FRO	−33/−34	83.64–83.91	10.554 ± 0.003
Neogloboquadrina atlantica l.s.	LO	−45	69.07–69.32	10.850 ± 0.002
Globoquadrina sp. 1	LO	−47/−48	66.17–66.37	10.895 ± 0.002
Neogloboquadrina atlantica l.s.	FO	−57/−58	51.52–51.87	11.121 ± 0.003
Neogloboquadrina group	2nd influx	−60	48.12–48.47	11.178 ± 0.003
Paragloborotalia mayeri	LO	−60	46.28–46.77	11.205 ± 0.004
Globorotaloides falconarae	FO	−64	37.95–38.00	11.360 ± 0.001
Globigerinoides subquadratus	LCO	−72/−73	28.40–28.83	11.539 ± 0.004
Neogloboquadrina group	FO	−79/−80	16.53–16.78	11.781 ± 0.002
Globoquadrina sp. 1	FO	−80/−81	15.53–15.68	11.800 ± 0.001
Calcareous nannofossil:				
Discoaster neohamatus	FO	−2	113.05–113.20	9.826 ± 0.003
Discoaster hamatus	FO	−16	100.10–100.32	10.150 ± 0.002
Helicosphaera stalis	FCO	−39	76.34–76.54	10.717 ± 0.002
Catinaster coalitus	FO	−40	75.29–75.44	10.738 ± 0.001
Helicosphaera walbersdorfensis	LCO	−40/−41	75.01–75.29	10.743 ± 0.003
Coccolithus miopelagicus	LRO	−52	61.37–61.57	10.977 ± 0.002
Discoaster kugleri	LCO	−75	24.78–25.03	11.604 ± 0.002
Discoaster kugleri	FCO	−83	11.08–11.48	11.889 ± 0.004

Astronomical ages are based on assuming constant sedimentation rates between the astronomically dated mid-points of the grey layers and sapropels given in Table 1. The error in the age is based on the uncertainty in the position of the events.

this suggests that *G. falconarae* and *C. parvulus* are homeomorphs but phylogenetically unrelated.

The *Globoquadrina* sp. 1 first occurrence (FO) is at 11.800 Ma. The species was not found in levels younger than 10.90 Ma. The *Globorotaloides falconarae* FO is at 11.360 Ma but it should be noted that this bio-event is not sharply defined.

5.1.2. Neogloboquadrina

We identified four types of *Neogloboquadrina*, i.e., *N. atlantica* (large- and small-sized), *N. acostaensis* s.s., and the so-called 4-chambered type. *N. atlantica* is characterised by an arched and generally intra-umbilical aperture. Large-sized representatives (Plate 2, 5–7) often show euhedral crystal growth. Small-sized *N. atlantica* (Plate 2, 1–4) has been previously reported under the label *Globigerina* aff. *pachyderma* (Tjalsma, 1971), *Globigerina continuosa* (Zachariasse, 1975), *Neogloboquadrina continuosa* (Zachariasse and Spaak, 1983; Chamley et al., 1986), and primitive *Neogloboquadrina atlantica* (Poore, 1979).

Representatives of *N. acostaensis* s.s. (Plate 2, 10–12) conform to the definition of this species as given in Blow (1969), i.e., they have ≥4.5 chambers and a low-arched, extra-umbilical aperture with a distinct lip. The 4-chambered type (Plate 2, 8 and 9) has a medium- to low-arched extra-umbilical aperture with or without lip and generally 4 chambers.

Although our concept of *N. acostaensis* allows the inclusion of 4-chambered types, we preferred to count *N. acostaensis* s.s. and the 4-chambered type separately because it facilitates evaluating the common practice of equating the Serravallian/Tortonian boundary with the level at or close to the FO of *N. acostaensis*.

Morphological gradation between *N. atlantica*, the 4-chambered form, and *N. acostaensis* s.s. (Plate 3) and their similar coiling suggest that they represent variants of one single species with *N. atlantica* being the dominant form in the lower part of the section, whereas the two other types prevail in the upper part (Fig. 4). The virtual absence of *N. atlantica* in the upper part of the section, while flour-

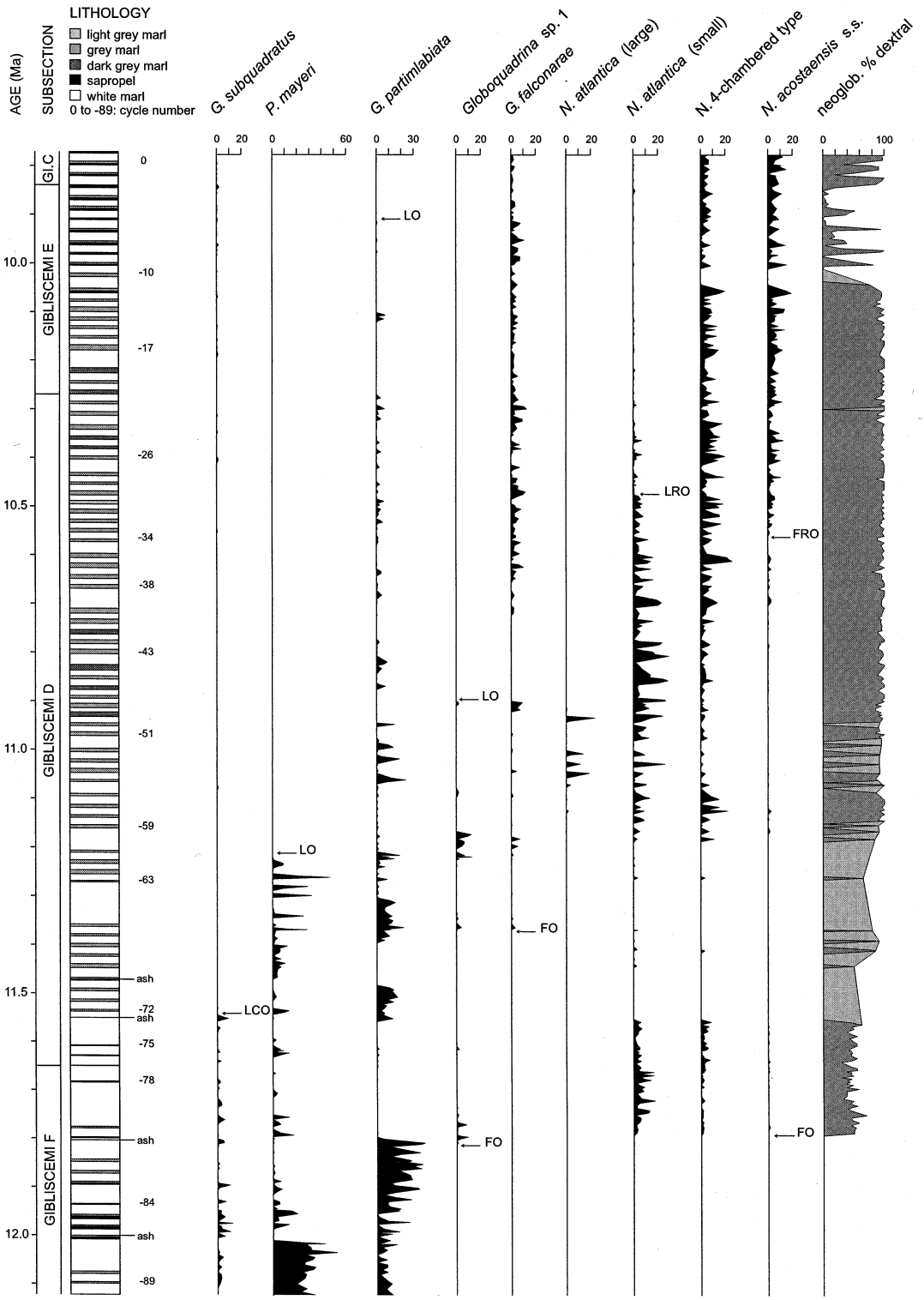
LITHOLOGY
light grey marl
grey marl
dark grey marl
sapropel
white marl
0 to -89: cycle number
AGE (Ma)
SUBSECTION
GI.C
GIBLISCEMI E
GIBLISCEMI D
GIBLISCEMI F
10.0
10.5
11.0
11.5
12.0
0
-10
-17
-26
-34
-38
-43
-51
-59
-63
ash
-72
ash
-75
-78
ash
-84
ash
-89
G. subquadratus
P. mayeri
G. partimlabiata
Globoquadrina sp. 1
G. falconarae
N. atlantica (large)
N. atlantica (small)
N. 4-chambered type
N. acostaensis s.s.
neoglob. % dextral
0 20
0 60
0 30
0 20
0 20
0 20
0 20
0 20
0 20
0 100
LO
LO
LO
FO
LRO
FRO
LCO
FO
FO

ishing at the same time in the high-latitude North Atlantic (Poore, 1979; Huddlestun, 1984), suggests a beginning of areal differentiation between *N. atlantica* and *N. acostaensis* (including the 4-chambered form). One might even speculate that this areal differentiation is attended by speciation, which would qualify *N. atlantica* as the immediate ancestor of *N. acostaensis*.

The origin of the group of neogloboquadrinids is still an unsolved question. Most authors follow Blow (1959) who considered *Globorotalia continuosa* (described by Blow from Zone N14 in Venezuela) to be the ancestral form of all other neogloboquadrinid species. However, the taxonomic status of this species is doubtful since this species is suspected to be a 4-chambered variant of *Paragloborotalia mayeri* (Bolli and Saunders, 1985). If true, then it would be an unsuitable candidate as ancestor of the neogloboquadrinids because *P. mayeri* is spinose (see Plate 4, 3), whereas neogloboquadrinids are non-spinose. The earliest neogloboquadrinids are known from the late-Middle Miocene in the North Atlantic region (Poore, 1979; Huddlestun, 1984; Zachariasse and Aubry, 1994). These earliest representatives are immigrants which must have come from regions north of Iceland since the earliest spreading of this group in the tropical region is in the early-Late Miocene (Zachariasse and Aubry, 1994; Chaisson and Pearson, 1997).

The overall resemblance between *N. atlantica* and some morphotypes within the species *Globoquadrina* sp. 1 (Plate 1, 7) might suggest that *N. atlantica* originated from the latter species in the Greenland–Iceland–Norwegian (GIN) seas or the Arctic Basin before they both invaded the North Atlantic region during the late-Middle Miocene. Even the North Pacific cannot be excluded as possible birth-place of the neogloboquadrinids since *N. atlantica* has recently been found also in middle Pliocene sediments from the North Pacific (Dowsett and Ishman, 1995). Unfortunately, this hypothesis remains untested due to the lack of Middle Miocene planktonic foraminiferal data from these regions.

In their Middle to Late Miocene planktonic foraminiferal study of the Mediterranean, Foresi et al. (1998) do not mention *N. atlantica* and suggest that what we labelled as *N. atlantica* is close to *G. falconarae*. Furthermore, they suggest an evolution from *G. falconarae* via *N. continuosa* to *N. acostaensis*. Based on their figures, however, their *N. continuosa* seems to correspond to our 4-chambered form, which in our opinion cannot be linked with *G. falconarae*. The above discussion is illustrative for the general lack of taxonomic consensus within the late-Middle Miocene group of *Neogloboquadrina* and our poor understanding of their origin and phylogeny.

The *Neogloboquadrina* FO in the Mediterranean is at 11.781 Ma. They are continuously present albeit in low percentages between 11.781 and 11.546 Ma. Rare and scattered occurrences are recorded between 11.546 and 11.178 Ma. From 11.178 Ma they become a major faunal constituent, being more frequent in sapropels than in homogeneous intervals (E. Turco, unpubl. data).

Coiling (based on $\geq$20 neogloboquadrinids) exhibits some biostratigraphically useful changes, being random between 11.781 and 11.546 Ma and persistently to the right (>80%) between 11.178 and 10.011 Ma. Large and rapid coiling changes occur as from 10.011 Ma to the top of the section at 9.777 Ma. Earlier work has shown that coiling is to the right again from 9.77 to 9.55 Ma (Krijgsman et al., 1995). These coiling changes have biostratigraphic potential since the change from random to right coiling has also been reported from the high-latitude North Atlantic (Huddlestun, 1984), while the rapid changes between 10.01 and 9.77 Ma have recently been recorded from Crete (unpubl. data).

Fig. 4. Quantitative distribution patterns of planktonic foraminiferal marker species (as % of the total planktonic foraminiferal fauna) through time. Time series based on linear interpolation of sediment accumulation rate between astronomically dated sapropel/grey layer mid-points, following the tuning presented in Fig. 3 and ages listed in Table 1. The following acronyms are used to indicate events: *FO* (first occurrence); *LO* (last occurrence); *LCO* (last common occurrence); *FRO* (first regular occurrence); *LRO* (last regular occurrence). The position of these bio-events is based on a qualitative analysis. The position of only two events (*N. acostaensis* s.s. FO and *P. mayeri* LO) is maximally 4 samples off from their position based on the quantitative analysis. Dark grey shading in the neogloboquadrinid % dextral column indicates the % of dextrally coiled neogloboquadrinids in sample intervals where neogloboquadrinids are continuously present. Light grey shading denotes sample intervals in which neogloboquadrinids are (near)absent.

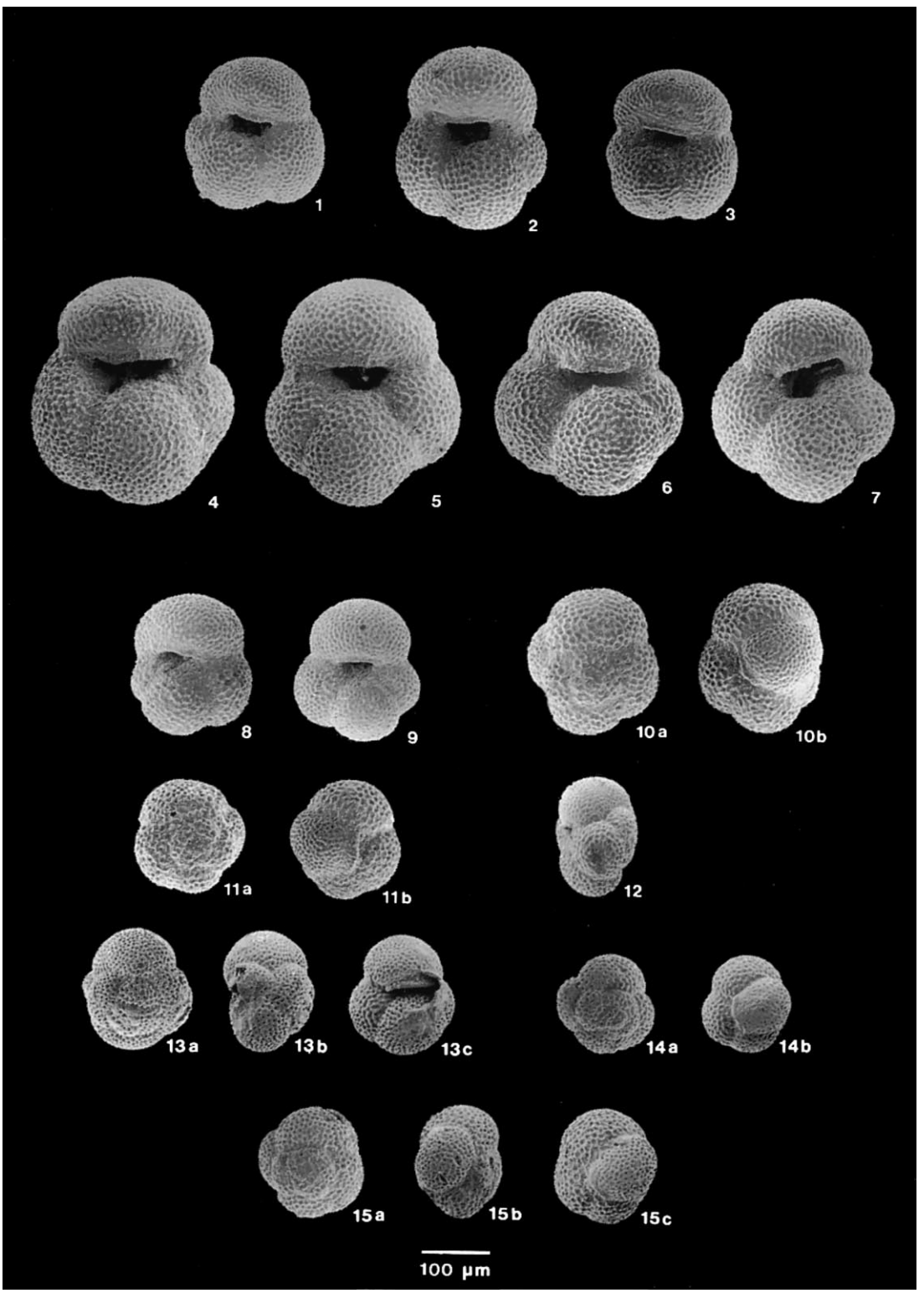
1
2
3
4
5
6
7
8
9
10a
10b
11a
11b
12
13a
13b
13c
14a
14b
15a
15b
15c
100 µm

Large-sized dominantly dextrally coiled *N. atlantica* are discontinuously present between 11.121 and 10.850 Ma, reaching peak abundances between 11.046 and 10.926 Ma. The occurrence of large-sized *N. atlantica* in the Mediterranean early-Late Miocene has previously been reported from northern Italy (Monte dei Corvi, Coccioni et al., 1994) and from Sicily (Sprovieri et al., 1996). The small-sized representatives occur over a much longer interval of time with the last regular occurrence (LRO) at 10.478 Ma (cycle −29).

N. acostaensis s.s. is present from the FO level of the neogloboquadrinids at 11.781 Ma, but starts to be continuously present in increasingly higher percentages at 10.554 Ma. The age of this first regular occurrence (FRO) level slightly pre-dates the LRO of *N. atlantica* at 10.478 Ma.

5.1.3. Paragloborotalia mayeri

The label *P. mayeri* is used here in the sense of Bolli and Saunders (1985) who consider *Paragloborotalia siakensis* and *Paragloborotalia continuosa* as junior synonyms of *P. mayeri*. The *P. mayeri* last occurrence (LO) is dated at 11.205 Ma.

5.1.4. Globigerinoides subquadratus

Trace occurrences in the upper part of the section might actually represent 3-chambered variants of *Globigerinoides obliquus*. The *G. subquadratus* last common occurrence (LCO) is at 11.539 Ma.

5.1.5. Globorotalia partimlabiata

This planoconvex globorotaliid has typically 4 to 5 chambers, an arched aperture, a subacute axial periphery, and a relatively coarsely perforated wall structure (Plate 4, 4–6). Our Mediterranean forms compare well with Early to early-Middle Miocene forms labelled *Globorotalia zealandica* by Poore (1979) in DSDP sites 407/408 west of Iceland. Whether these North Atlantic forms are truly conspecific with the species originally described from New Zealand or that *Globorotalia partimlabiata* is a more correct name requires further study, but it seems justified to postulate that the sudden arrival of *G. partimlabiata* in the Mediterranean during the late-Middle Miocene reflects the southward migration of *G. zealandica* sensu Poore (1979). Remarkable is that globorotaliids indistinguishable from *G. partimlabiata* invaded the low latitudes of the Southern Hemisphere at about the same time (Zachariasse, 1992). No such forms have been reported from the equatorial region, suggesting that the Southern Hemisphere forms and *G. partimlabiata* might represent homeomorphs which evolved in the mid- to high-latitudes of both hemispheres from different ancestral species.

The *G. partimlabiata* LO is dated at 9.913 Ma. Comparison with Chamley et al. (1986) indicates that the actual FO level of this species in the Mediterranean is slightly below the base of section Gibliscemi.

5.2. Calcareous nannofossils

Results of biostratigraphic analyses on calcareous nannofossil assemblages are presented in Fig. 5. The strategy of combining quantitative analytical methods with high-resolution sampling resulted in a detailed biostratigraphy, which essentially confirmed the validity of the regional zonal scheme proposed by Fornaciari et al. (1996), and which records even weak biostratigraphic signals.

497 smear slides were prepared from unprocessed samples using standard techniques and were examined under the light microscope. Calcareous nannofossils are generally abundant; their preservation is variable, and partially dissolved or overgrown assemblages are repeatedly found. Only a few samples (4) are completely barren of nannofossils.

The quantitative data were collected using count-

Plate 1

1–7. *Globoquadrina* sp. 1: 1–3 umbilical view, sample It 18.573; 4–7 umbilical view, sample It 15.536.

8–12. *Globorotaloides falconarae* Giannelli and Salvatorini: 8 and 9 umbilical view, sample It 14.837; 10a and 11a spiral view, and 10b and 11b umbilical view; sample It 15.531; 12 axial view, sample It 14.837.

13–15. *Catapsydrax parvulus* Bolli, Loeblich and Tappan: 13a and 15a spiral view, 13b and 15b axial view, and 13c and 15c umbilical view; 14a spiral view, 14b umbilical view. Sample TTOC 193.125 (*G. fohsi peripheroronda* Zone, Bolli 1957), Cipero Formation, Trinidad.

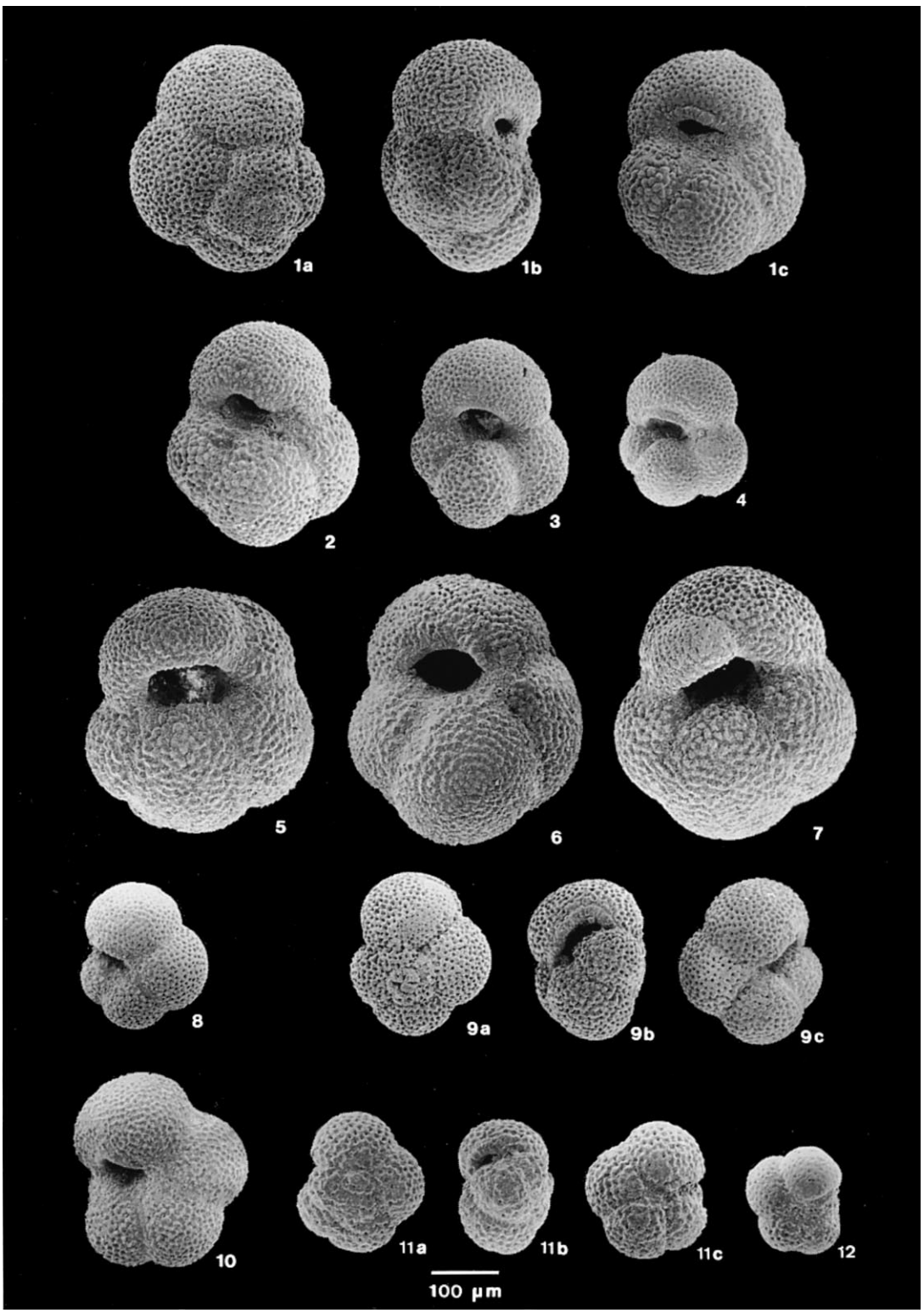
1a
1b
1c
2
3
4
5
6
7
8
9a
9b
9c
10
11a
11b
11c
12
100 µm

ing techniques of Backman and Shackleton (1983) and Rio et al. (1990a) according to the following methods: (1) counting the number of specimens of the index species or taxonomic group per unit area of the slide; and (2) counting the index species relative to a prefixed number of taxonomically related forms.

Method (1) was applied to obtain distribution patterns of the discoasterid group (genera *Discoaster* and *Catinaster*), of selected species within this group, and for evaluating the abundance of *Coccolithus miopelagicus*. Method (2) was applied for evaluating abundances of *Helicosphaera walbersdorfensis* and *Helicosphaera stalis*. The reader is referred to Theodoridis (1984) and Perch-Nielsen (1985) for the taxonomy of the calcareous nannofossil species considered in this paper. Advantages and limits of the application of the data-collecting methods are discussed in Backman and Shackleton (1983) and Rio et al. (1990b), to which the reader is referred as well.

The distribution patterns of the selected calcareous nannofossil species are shown in Fig. 5. Most of them are index species for the Middle and Late Miocene in the low-latitude ocean and/or the Mediterranean but in section Monte Gibliscemi they do not always provide a robust biostratigraphic signal. Nevertheless, some of the more scattered occurrences are discussed here as well, due to their biostratigraphic and biochronologic significance.

On the basis of the distribution patterns, the following biohorizons, reported in stratigraphic order, are identified: FCO (first common occurrence) and LCO (last common occurrence) of *Discoaster kugleri*; LRO (last regular occurrence) of *C. miopelagicus*; LCO of *H. walbersdorfensis*; and FCO of *H. stalis*.

The occurrences or distribution patterns of the following additional species are also discussed: presence of *Catinaster coalitus* and *Discoaster micros*; presence of *Discoaster bellus* gr., *Discoaster hamatus*, and *Discoaster neohamatus*; presence of *Discoaster brouweri*; distribution pattern of *Discoaster exilis*. Data on the abundance of other secondary *Discoaster* species (*D. variabilis, D. intercalaris* and *D. bollii*) are not included in the discussion.

The biostratigraphic and biochronologic reliability of the biohorizons in terms of degree of reproducibility, of correlatability among distant and/or different facies/sections, and of isochrony and diachrony is discussed and clarified in Raffi et al. (1995), Fornaciari et al. (1996) and Backman and Raffi (1997). Age estimates of the biohorizons were obtained through calibration to the orbitally tuned cyclostratigraphy, providing a nannofossil astrobiochronology for the Middle and Late Miocene in the Mediterranean (see Table 2).

5.2.1. The discoasterid group

Discoasterids are recorded in highly variable, but generally low abundances throughout the section. High-frequency variations are present with higher abundances of discoasterids in the grey marl layers and associated sapropels. A variable degree of dissolution of other elements of the nannofossil assemblage (i.e., helicoliths and placoliths) is observed in these layers. Discoasterids are known to be dissolution-resistant and their percentages may be used as an indicator of the dissolution intensity (see references in Rio et al., 1990b). The high-frequency variations in discoasterid abundances are therefore interpreted as a preservational signal. The effect of dissolution decreases in the upper part of the section where the general preservation state of nannofossil assemblages ameliorates. In this interval abundance variations in the discoasterids could reflect a productivity signal.

The discoasterid distribution pattern shows long-term variations in abundance as well. In the lower part of the section (up to about 11.6 Ma) discoast-

Plate 2

1–4. *Neogloboquadrina atlantica* (small-sized): 1a spiral view, 1b axial view, and 1c umbilical view; sample It 18.575; 2–3 umbilical view, sample It 18.575; 4 umbilical view, sample Gib D 21.

5–7. *Neogloboquadrina atlantica* (large-sized), umbilical view, sample It 15.490.

8, 9. *Neogloboquadrina* 4-chambered type: 8 umbilical view, sample It 18.575; 9a spiral view, 9b axial view, and 9c umbilical view; sample It 18.575.

10–12. *Neogloboquadrina acostaensis* s.s.: 10 and 12 umbilical view, sample It 18.575; 11a spiral view, 11b axial view, and 11c umbilical view; sample It 18.575.

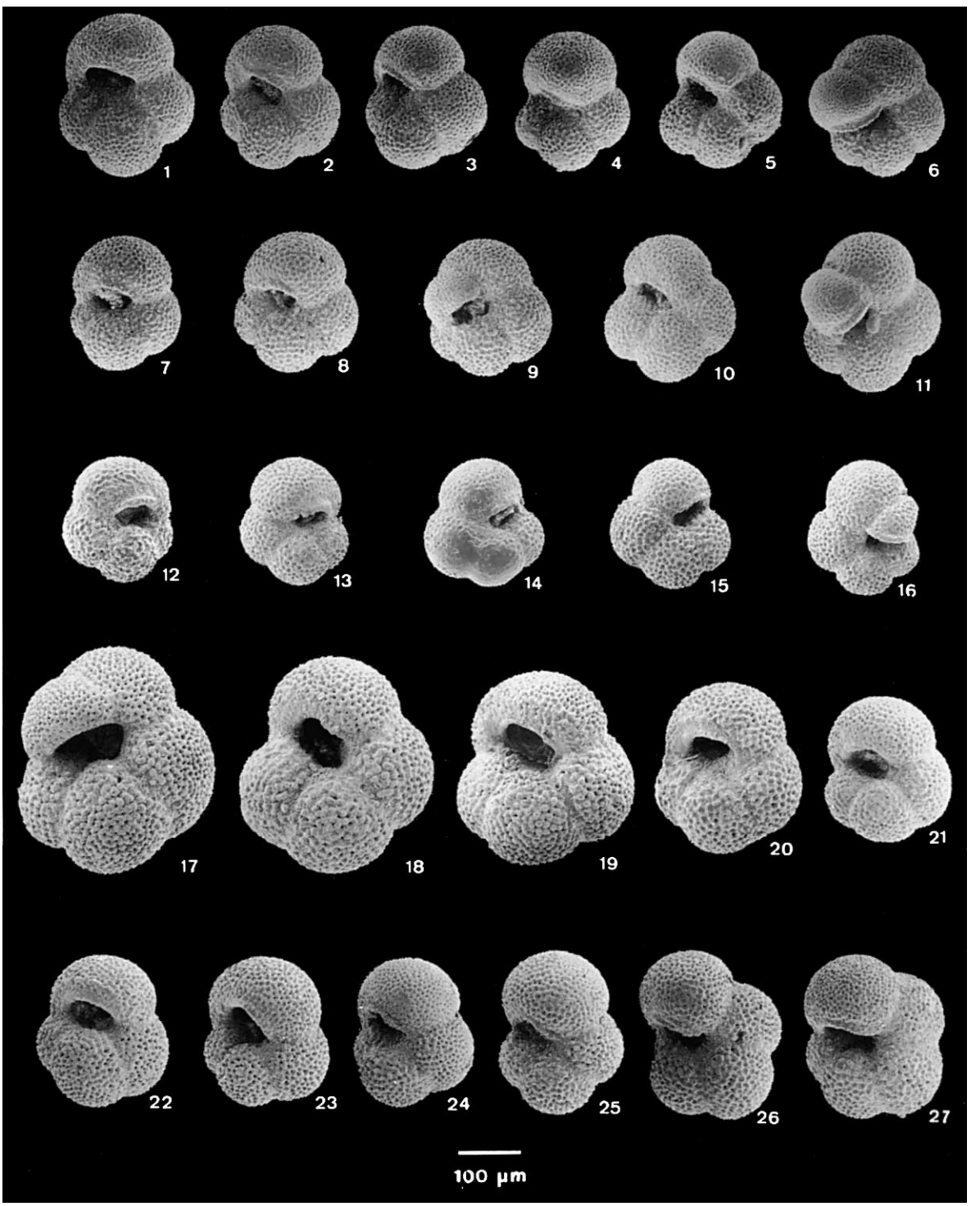
1
2
3
4
5
6
7
8
9
10
11
12
13
14
15
16
17
18
19
20
21
22
23
24
25
26
27
100 µm

erids are consistently present, although with varying abundances, whereas they are very rare, intermittently distributed and often absent from about 11.6 to 10.8 Ma. Above this interval discoasterids increase again. These intervals with generally low abundance or absence of discoasterids at different levels could indicate variations in productivity. The abundance of discoasterids is considered to be influenced by productivity (Chepstow-Lusty et al., 1989; Chepstow-Lusty et al., 1992); low abundance or absence of discoasterids are associated with high productivity, as observed in Pliocene sections in the Atlantic Ocean (Chepstow-Lusty et al., 1989; Chepstow-Lusty et al., 1992), and in the Late Miocene of the eastern equatorial Pacific (Raffi and Flores, 1995).

5.2.2. FCO and LCO of Discoaster kugleri

The biostratigraphic value of *D. kugleri* was clarified by Raffi et al. (1995) in the study of sedimentary successions from tropical ocean environments, where an interval of common and continuous presence of *D. kugleri* was calibrated magnetostratigraphically to Chron C5r (from the lower part of C5r to C5r.2n). In the western equatorial Atlantic the FCO and LCO of *D. kugleri* were astronomically calibrated and dated at 11.797 and 11.554 Ma, respectively (Backman and Raffi, 1997). A detailed re-examination of the calibration reported by Backman and Raffi (1997) revealed an inconsistency between the timescale used for nannofossil age calibration and the timescale published by Shackleton and Crowhurst (1997), exactly in the interval where the FCO and LCO of *D. kugleri* are recorded (Backman and Raffi inadvertently did not use the final version of Shackleton and Crowhurst's timescale). The respective ages for the FCO and LCO of *D. kugleri* are 11.876 ± 0.003 and 11.597 ± 0.005 if the updated orbitally tuned timescale is used for age calibration (Fig. 6).

Although the interval of abundance of *D. kugleri* in the Middle Miocene has a wide geographic distribution (Raffi et al., 1995; Backman and Raffi, 1997), *D. kugleri* is generally rare in the Mediterranean, and therefore considered biostratigraphically to be of no or only very limited value (see discussion in Fornaciari et al., 1996). For this reason it is not included as a (sub)zonal marker in the Middle Miocene Mediterranean zonation by Fornaciari et al. (1996). The short duration of the interval of common and continuous presence of *D. kugleri* in combination with a low(er)-frequency sampling may explain the failure to record it in other Mediterranean sections. Results of the analyses on the high-resolution sample set from Monte Gibliscemi show that the biostratigraphic signal provided by *D. kugleri* (Plate 5, 1–5) is clear and that both the FCO and LCO are easily identified (Fig. 5). Their respective age estimates of 11.889 and 11.604 Ma (Table 2) are in almost perfect agreement with the astronomical ages obtained for the same events in the western equatorial Atlantic (Backman and Raffi, 1997). An emendation of the Middle to early-Late Miocene calcareous nannofossil zonation for the Mediterranean (Fornaciari et al., 1996) with the erection of a *D. kugleri* Subzone within the *H. walbersdorfensis* Partial-range Zone (MNN7 of Fornaciari et al., 1996) is obvious and proposed here. The additional use of the *D. kugleri* datums permit subdividing MNN7 into MNN7a (from the *C. premacintyrei* LCO to the *D. kugleri* FCO), MNN7b (from the *D. kugleri* FCO to the *D. kugleri* LCO) and MNN7c (from the *D. kugleri* LCO to the *H. walbersdorfensis* LCO).

5.2.3. LRO of Coccolithus miopelagicus

The biostratigraphic value of the *C. miopelagicus* last occurrence datum has been recognised in oceanic sediments, although a slight diachroneity

Plate 3

1–6. Variation from *Neogloboquadrina atlantica* (small-sized) to *Neogloboquadrina acostaensis* s.s., umbilical view, sample Gib D 1.
7–11. Variation from *Neogloboquadrina atlantica* (small-sized) to *Neogloboquadrina acostaensis* s.s., umbilical view, sample Gib D 21.
12–16. Variation from *Neogloboquadrina atlantica* (small-sized) to *Neogloboquadrina acostaensis* s.s., umbilical view, sample Gib D 21.
17–21. Variation from *Neogloboquadrina atlantica* (large-sized) to *Neogloboquadrina atlantica* (small-sized), umbilical view, sample It 15.503.
22–27. Variation from *Neogloboquadrina atlantica* (small-sized) to *Neogloboquadrina acostaensis* s.s., umbilical view, sample It 15.375.

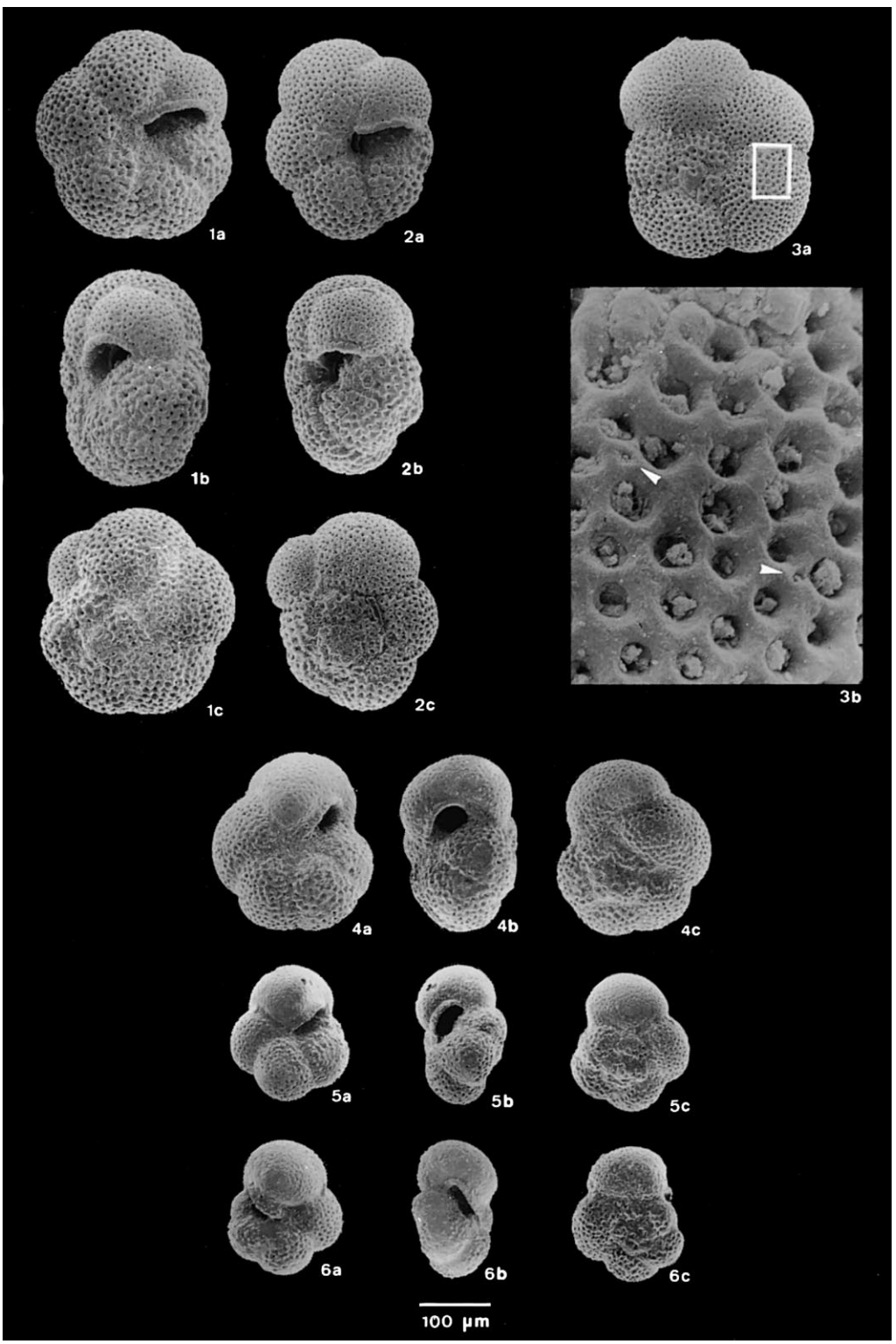
1a
2a
3a
1b
2b
3b
1c
2c
4a
4b
4c
5a
5b
5c
6a
6b
6c
100 µm

was inferred for this event between low and middle latitudes (Raffi et al., 1995). Backman and Raffi (1997) demonstrated that the inferred diachroneity actually exists between the eastern equatorial Pacific and the Atlantic (Atlantic mid-latitudes and western equatorial region).

The last occurrence of *C. miopelagicus* has been documented in detail also in the Mediterranean, where the species is well-represented, and Fornaciari et al. (1996) defined its last continuous presence which occurs just below the disappearance level of *H. walbersdorfensis*. Although it is an easily detectable event it is not used in the proposed Mediterranean zonal system.

The distribution pattern of *C. miopelagicus* (Figs. 5 and 6; Plate 5, 6 and 7) in section Gibliscemi shows affinity with its distribution in the western equatorial Atlantic (Backman and Raffi, 1997) and mid-latitude Atlantic DSDP Site 608 (Olafsson, 1991; Gartner, 1992). At this latter site the disappearance event of *C. miopelagicus* occupies the same stratigraphic position relative to the *D. hamatus* first occurrence (FO; sensu Olafsson, 1991) as in section Gibliscemi.

In the Mediterranean we define this event as the *C. miopelagicus* LRO because of the occurrence of rare and scattered specimens higher in the section. The *C. miopelagicus* LRO dated at 10.977 Ma coincides approximately with its last occurrence (LO) in the equatorial Atlantic dated at 10.941 Ma (Fig. 6), indicating that our *C. miopelagicus* LRO represents a (near-)synchronous event between the mid-latitudes (Mediterranean and Site 608) and the low-latitude Atlantic (Ceara Rise). The LO in the equatorial Pacific, however, is much younger (10.39 Ma) and may represent the actual extinction of the species.

5.2.4. LCO of Helicosphaera walbersdorfensis and FCO of Helicosphaera stalis

The distribution patterns of *H. walbersdorfensis* and *H. stalis* (Fig. 5) are in agreement with the distributions reported by Fornaciari et al. (1996). Abundances of the helicoliths were quantitatively evaluated in the lower part of the section and in the interval from 47 to 85 m. Above this interval, helicoliths are discontinuously present, and their abundance could not be evaluated due to their rareness in most of the samples.

H. walbersdorfensis (Fig. 5; Plate 5, 13) is present from the basal interval of the section, where it is relatively common to abundant (percentages are generally >30% of the helicolith assemblage). *H. stalis* (Plate 5, 14) occurs sporadically, with rare specimens, along the upper range of *H. walbersdorfensis*. We did not observe a clear reversal in abundance between the two taxa as expected. Between 10.743 and 10.717 Ma, two biohorizons, LCO of *H. walbersdorfensis* and FCO of *H. stalis* can be recognised. Actually, *H. stalis* shows consistent abundances only sporadically within its lower range, and in most of the samples it is rare or absent.

Detailed distribution patterns of these taxa outside the Mediterranean, as well as calibrations of the associated biohorizons, are not available because these taxa are very rare in the open ocean. The astronomical age estimates (Table 2) indicate that the two events in the Mediterranean occurred concomitantly with the appearance of the marker *Catinaster coalitus* in the oceans.

5.2.5. Presence of Catinaster coalitus and Discoaster micros

C. coalitus is a well-known marker species in low-latitude biostratigraphic schemes (Bukry, 1973, 1978). Like other representatives of the genus *Catinaster*, *C. coalitus* is consistently present in the

Plate 4

1, 2. *Paragloborotalia mayeri* (Cushman and Ellisor): 1a umbilical view, 1b axial view, and 1c spiral view; sample It 18.516; 2a umbilical view, 2b axial view, and 2c spiral view; sample It 15.548.

3. *Paragloborotalia mayeri* (Cushman and Ellisor): 3a spiral view, 3b detail of wall structure; arrows point to spine holes. Sample TTOC 215.660 (*G. foshi robusta* Zone, Bolli 1957) Cipero Formation, Trinidad.

4–6. *Globorotalia partimlabiata* Ruggieri and Sprovieri: 4a umbilical view, 4b axial view, and 4c spiral view; sample It 18.553; 5a umbilical view, 5b axial view, and 5c spiral view; sample It 15.503; 6a umbilical view, 6b axial view, and 6c spiral view; sample It 14.803.

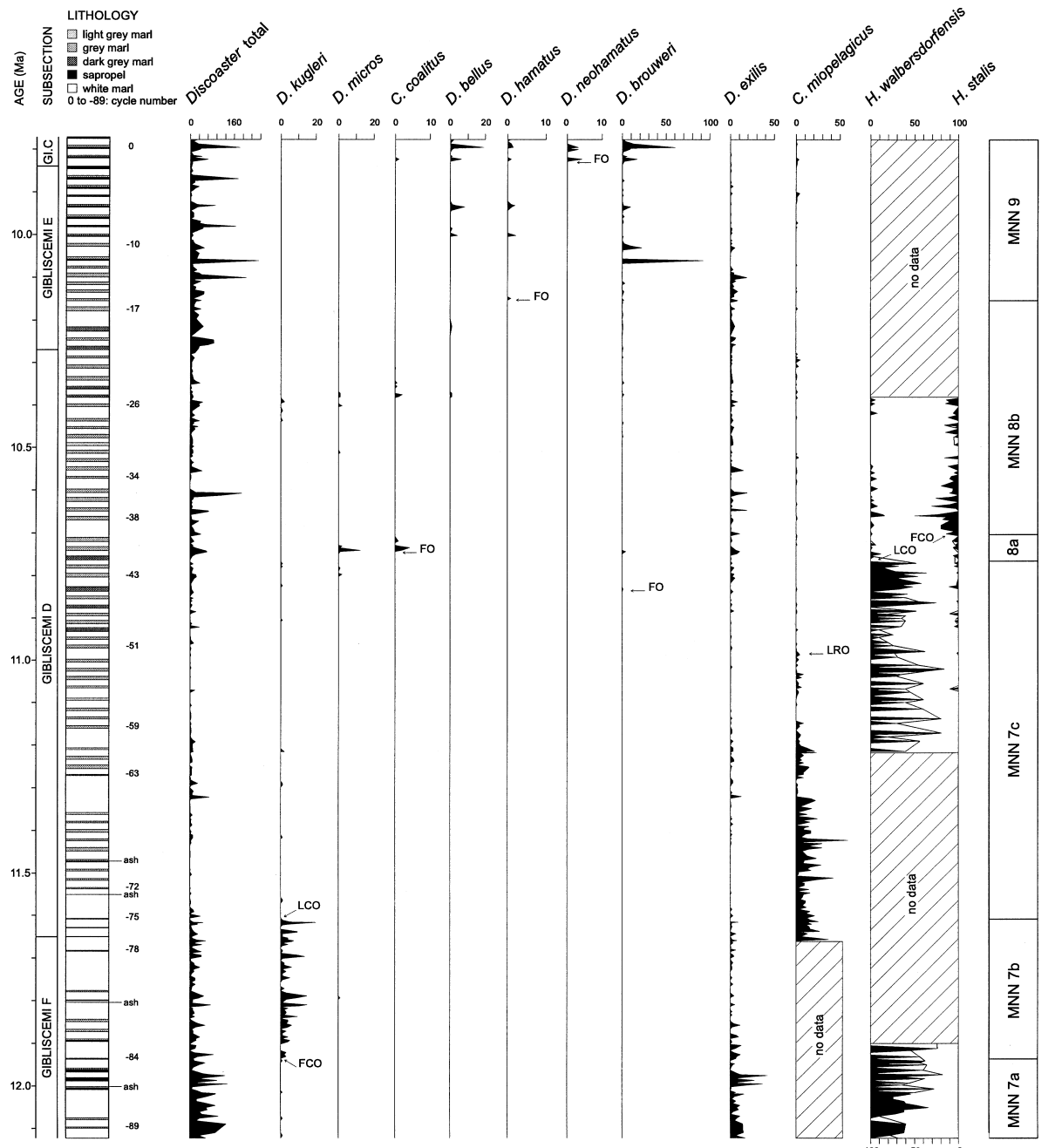

Fig. 5. Quantitative distribution patterns of calcareous nannofossil marker species through time based on counting the number of specimens of the index species or taxonomic group per unit area of the slide (mm^{-2}; i.e., *C. miopelagicus* and *Discoaster* species), or on counting the index species relative to a prefixed number of taxonomically related forms (*Helicosphaera* species). The following acronyms are used to denote events: *FO* (first occurrence); *FCO* (first common occurrence); *LCO* (last common occurrence); *LRO* (last regular occurrence). Biozonation (*MNN* zones) modified after Fornaciari et al. (1996).

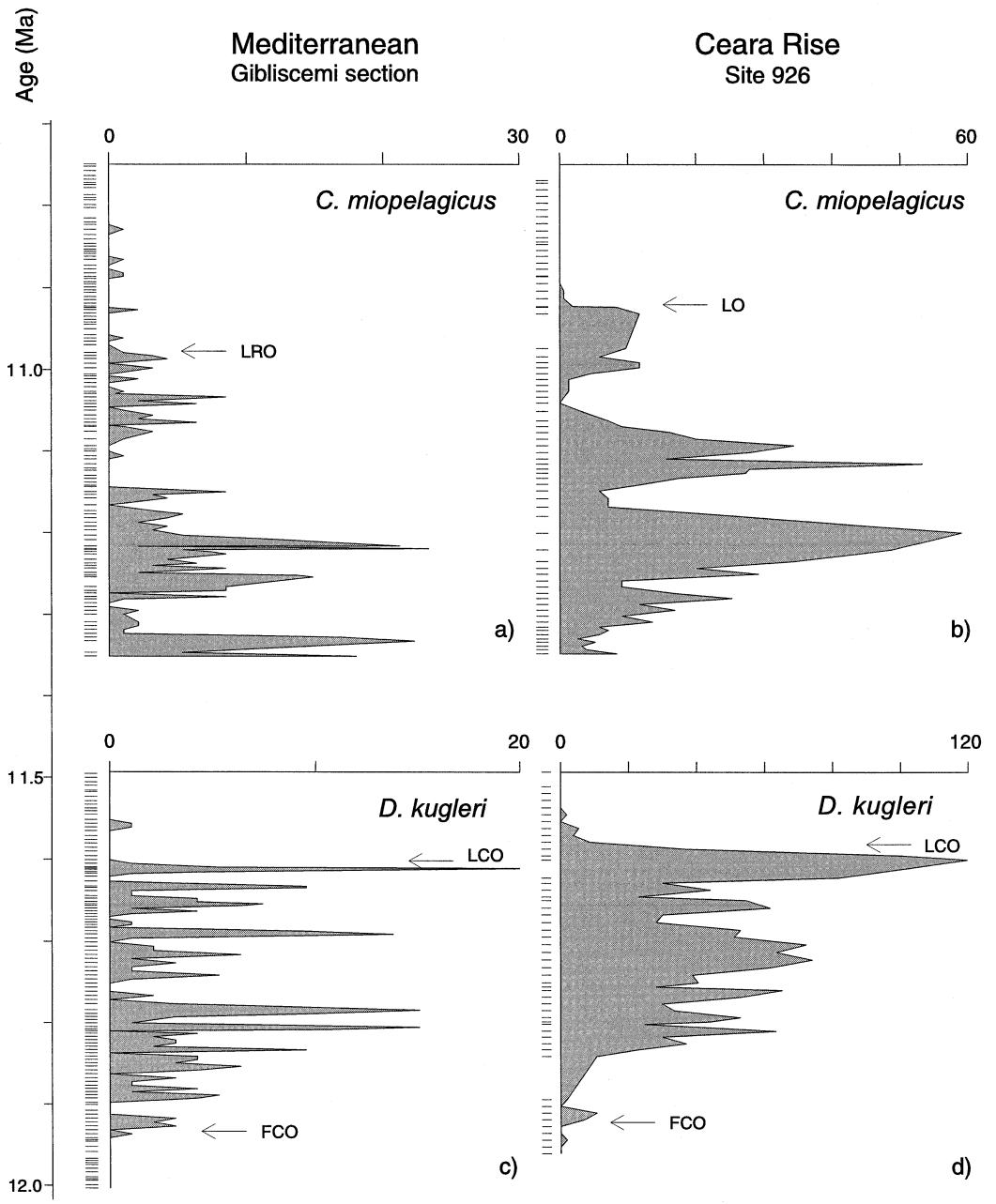

Fig. 6. Comparison of the quantitative distribution patterns of *C. miopelagicus* and *D. kugleri* at Ceara Rise and in the Mediterranean. Time series based on the independently established astronomical chronologies for Ceara Rise (Shackleton and Crowhurst, 1997) and Monte Gibliscemi (this study).

low-latitude assemblages, whereas it is known to be scattered to absent at mid-latitudes such as at DSDP Site 608 (Olafsson, 1991) and in the Mediterranean (Theodoridis, 1984; Fornaciari et al., 1996). It seems that the distribution of these forms is controlled by productivity conditions, because *Catinaster* specimens are very rare or absent even at low-latitude sites where high productivity influenced carbonate

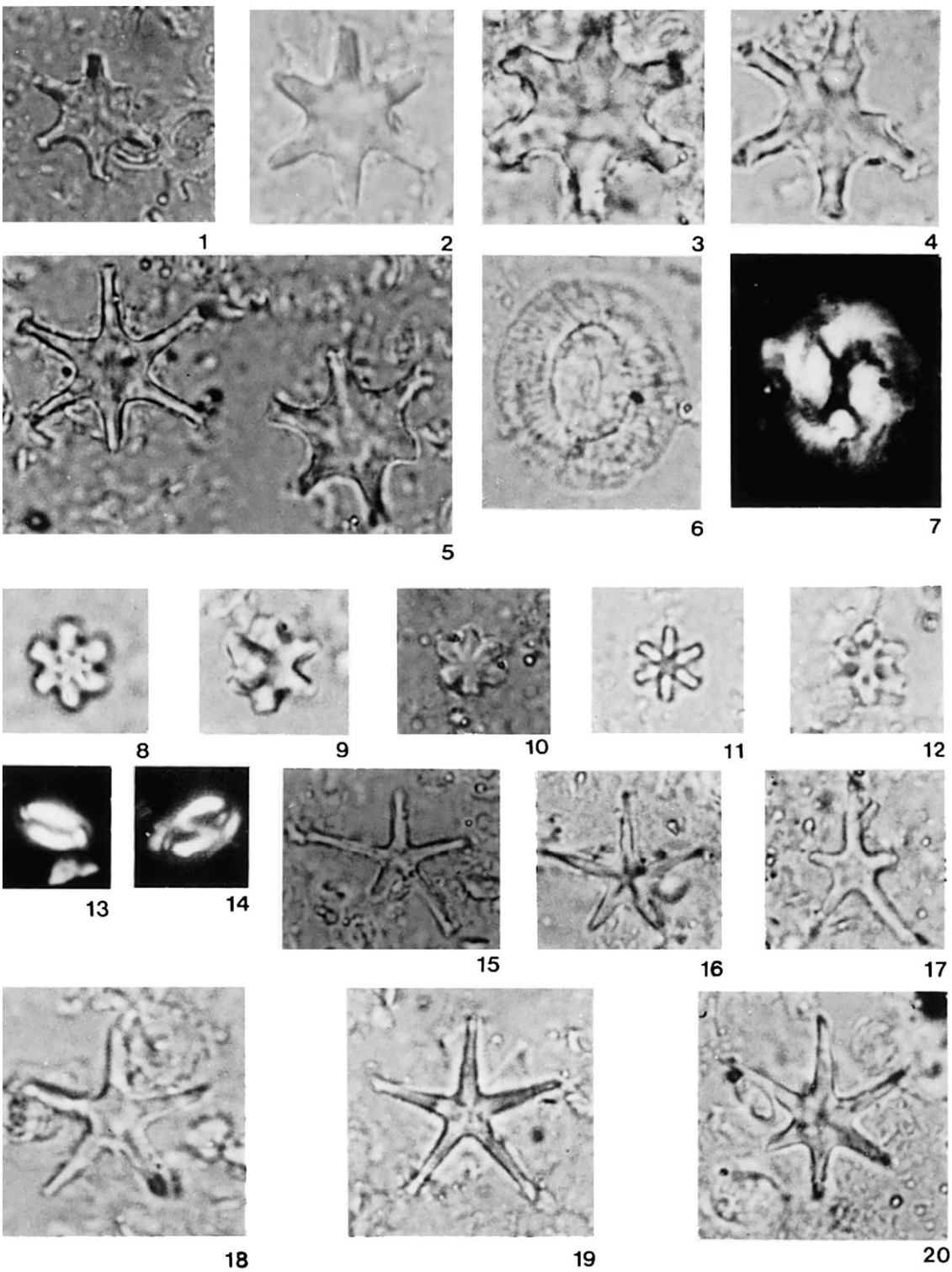
1
2
3
4
5
6
7
8
9
10
11
12
13
14
15
16
17
18
19
20

accumulation (e.g., in the eastern equatorial Pacific; Raffi and Flores, 1995).

Observations in the high-resolution sample set of Monte Gibliscemi section allowed to detect very rare specimens of *C. coalitus* (Plate 5, 10–12) in spot samples from two short stratigraphic intervals (Fig. 5). The lowermost observed specimens occur together with *Discoaster micros* (Plate 5, 8 and 9), a discoasterid from which the genus *Catinaster* is considered to have evolved (Raffi et al., 1998). Although the distribution pattern does not point to a reliable (reproducible) biostratigraphic signal, it is interesting to note that the age assignment for the *C. coalitus* FO at Monte Gibliscemi section (10.738 Ma) is in agreement with the astronomical age for the first appearance of this species in the western equatorial Atlantic (at 10.794 Ma).

5.2.6. Presences of Discoaster bellus gr., Discoaster hamatus and Discoaster neohamatus

As for the marker species *C. coalitus*, the taxa *D. hamatus* and *D. bellus* gr. (Plate 5, 15–19) do not provide a robust biostratigraphic signal at Monte Gibliscemi section (Fig. 5). Although these two 5-ray discoasterid species are rare in the nannofossil assemblages of the Mediterranean Middle to Late Miocene, Fornaciari et al. (1996) already showed that their FO horizons can be applied as regional zonal boundaries.

The appearances of these distinctive discoasterids provide reliable events in the open ocean (Raffi et al., 1995), where the *D. bellus* gr. FO slightly precedes that of *D. hamatus*. The same distribution was recorded in the western equatorial Atlantic, where the *D. hamatus* FO was astronomically dated at 10.47 Ma (Backman and Raffi, 1997). Their magnetostratigraphically calibrated positions were precisely established in the middle part of Subchron 5n.2n in the eastern tropical Pacific (Leg 138 sites, Raffi et al., 1995), and in the North Atlantic (Site 608: Olafsson, 1991; Gartner, 1992), where the first rare specimens of *D. hamatus* were detected within 5n.2n as well; at this site, the taxon increases in abundance close to the top of Chron 5n, with an approximate age of 10.05–10.06 Ma (using the timescale of Hilgen et al., 1995). The astronomical age of 10.150 Ma obtained for the lowermost observed specimens of *D. hamatus* at Gibliscemi is, despite its highly sporadic occurrence in the section, in agreement with the re-calibrated age obtained for the *D. hamatus* FO as defined by Olafsson (1991) at Site 608. This biohorizon as recorded at mid-latitudes is clearly delayed with respect to the *D. hamatus* appearance in the equatorial areas of the Pacific and Atlantic oceans. In the western equatorial Atlantic, the *D. hamatus* appearance is dated astronomically at 10.476 Ma (Backman and Raffi, 1997), and correlates reasonably well with the level of the lowermost specimens of the species observed at Site 608 (Olafsson, 1991).

D. neohamatus FO is a distinct event in some oceanic areas where the species is well represented (Raffi et al., 1995); it seems diachronous between different ocean basins, as suggested by the variable distribution patterns of the species observed in different environmental settings. Rare, sporadic specimens of *D. neohamatus* (Plate 5, 20) were found in the upper part of the Monte Gibliscemi section, in correspondence with the scattered presence of *D. hama-*

Plate 5

Specimens in 1–12, 15–20: ×2500; in 13, 14: ×2700.

1–4. *Discoaster kugleri* Martini and Bramlette, parallel light: 1 and 4 sample It 18.593B; 2 sample It 18.592; 3 sample Gib D 21.
5. *Discoaster kugleri* Martini and Bramlette and *Discoaster exilis* Martini and Bramlette, parallel light, sample It 18.593B.
6, 7. *Coccolithus miopelagicus* Bukry, sample It 18.593B: 6 parallel light; 7 crossed nicols.
8. *Discoaster micros* Theodoridis, parallel light, sample It 15.422.
9. *Discoaster micros–Catinaster* intergrade, parallel light, sample It 15.422.
10–12. *Catinaster coalitus* Martini and Bramlette (primitive morphotypes), parallel light, sample It 15.422.
13. *Helicosphaera walbersdorfensis* (Muller), crossed nicols, sample It 15.527.
14. *Helicosphaera stalis* Theodoridis, crossed nicols, sample It 14.839.
15. *Discoaster bellus* gr., parallel light, sample It 14.839.
16. *Discoaster bellus* gr.–*Discoaster hamatus* intergrade, parallel light, sample It 14.840.
17–19. *Discoaster hamatus* Martini and Bramlette, parallel light: 17 and 19 sample It 14.840; 18 sample It 14.738.
20. *Discoaster neohamatus* Bukry and Bramlette; parallel light, sample It 14.738.

tus and the *D. bellus* gr. (Fig. 5). The lowermost observed specimen is at 113.20 m, corresponding to the astronomical age of 9.823 Ma. This weak biostratigraphic signal is in agreement with the *D. neohamatus* distribution at Site 608 (Gartner, 1992), where the species is recorded as very rare within the range of *D. hamatus*, in the upper part of Chron 5n.2n. In the equatorial Atlantic, *D. neohamatus* is rare within the range of *D. hamatus*, and increases in abundance between 9.80 and 9.77 Ma (Backman and Raffi, 1997); this age is in agreement with the age obtained at Monte Gibliscemi, considering the scattered distribution of the species.

Concomitantly with *D. neohamatus*, an increase in abundance of *D. brouweri* is recorded in the Gibliscemi section. The distribution of the species is consistent with that observed outside the Mediterranean, even though it is influenced by local environmental conditions that seem to control discoasterid distribution patterns. In fact the pattern observed at Monte Gibliscemi (the lowermost observed specimen is at 75.29 m, corresponding to the age of 10.740 Ma) is similar to that of the equatorial Atlantic (Backman and Raffi, 1997), where *D. brouweri* appears at about 10.7 Ma, is rare in the lower part of its range and increases in abundance when *D. neohamatus* increases.

5.2.7. Distribution pattern of Discoaster exilis

The distribution range of *D. exilis* is reported here for comparing the Mediterranean data with the final range of the species as recorded in the open ocean. Raffi et al. (1995) showed that the *D. exilis* LO is an event controlled by environmental conditions and biogeography, and occurs in the interval encompassing the appearance level of *D. hamatus* (between the top of Zone CN6 and the lowermost part of Zone CN7). The biostratigraphic signal provided by *D. exilis* — irrespective whether it represents the local extinction or a decline in abundance — together with the appearance of the 5-ray discoasterids marks a significant turnover in the nannofossil assemblage in the early-Late Miocene. The event is even recorded in the 'environmentally' controlled assemblages of Monte Gibliscemi where its distribution pattern is in good agreement with that observed in the open ocean (Raffi et al., 1995), particularly so in the western equatorial Atlantic where the species gradually disappears close to the *D. hamatus* FO (Raffi, unpubl. data).

6. Magnetostratigraphy

The Gibliscemi section was sampled for magnetostratigraphic purposes with 5 levels per sedimentary cycle, which corresponds to an average 4000-year resolution. Standard paleomagnetic cores were drilled in the field from 294 levels; unfortunately some sapropelitic intervals were impossible to drill. The natural remanent magnetisation (NRM) was measured on a 2G Enterprises horizontal cryogenic magnetometer equipped with DC SQUIDS. One specimen per sampling level was thermally demagnetised up to temperatures of 360–390ºC in a magnetically shielded, laboratory-built furnace using temperature steps of 30–50ºC. Heating the samples at temperatures above 400ºC resulted in a sudden increase of susceptibility and the creation of a viscous remanent magnetisation. This is related to the presence of pyrite which oxidises into magnetite at temperatures higher than 400ºC, a common feature in suboxic to anoxic sediments and also observed in the younger part of Monte Gibliscemi (Krijgsman et al., 1995).

NRM intensities of the samples are generally low (50–300 μA/m), similar to the younger part of the Gibliscemi section (Krijgsman et al., 1995). Thermal demagnetisation revealed three types of Zijderveld diagrams: (1) diagrams with only a normal polarity component which was progressively demagnetised till 360ºC showing a linear decay towards the origin (Fig. 7a); these normal polarity components have approximately a present-day field direction before bedding tilt (tectonic) correction; (2) diagrams with a more or less randomly directed component passing the origin during demagnetisation (Fig. 7b); (3) diagrams which only show scatter (Fig. 7c). All three types of Zijderveld diagrams are (irregularly) observed throughout the entire section. Furthermore, thermal demagnetisation did not reveal reversed polarity components. Therefore, we have interpreted the normal polarity component as a (sub-recent) weathering-induced overprint and the randomly directed component as a secondary diagenetic overprint. Consequently, no reliable magnetostratigraphy

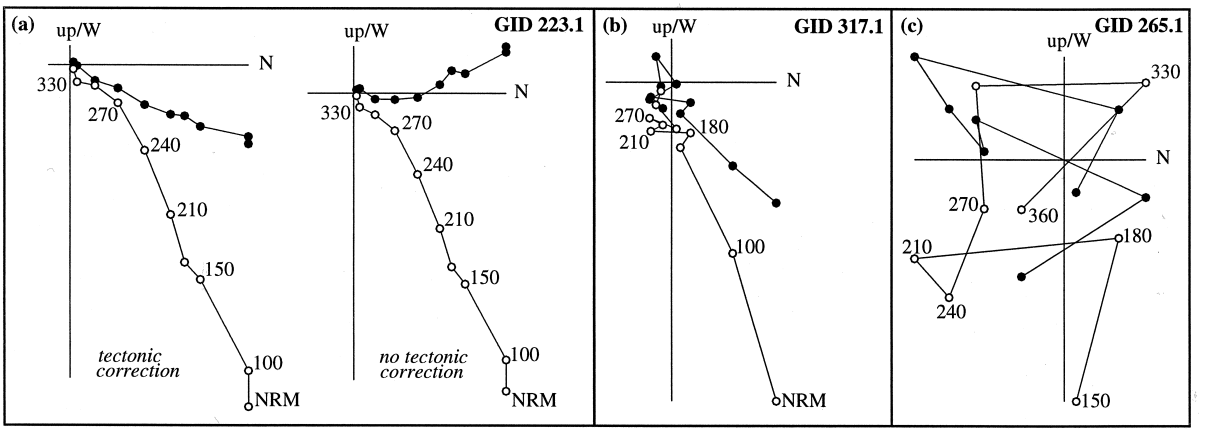

Fig. 7. Zijderveld diagrams of stepwise thermal demagnetisation of selected samples from the Gibliscemi D section. Solid (open) dots represent the projection of the NRM vector end-point on the horizontal (vertical) plane. Values represent temperature in ºC. (a) A normal component with a linear decay to the origin. Note that without tectonic correction this component has approximately a present-day field direction. (b) Diagram with a component that passes the origin. (c) Scatter diagram.

could be established for the downward extension of the Gibliscemi section.

7. Discussion

7.1. Comparison with other timescales

Calcareous plankton biostratigraphic data have been reported from several sections in the Mediterranean which span the Serravallian/Tortonian boundary but lack a direct first-order age control (e.g., Sprovieri et al., 1996; Foresi et al., 1998). The only exception is Monte dei Corvi which contains two volcanic ash layers that have been dated using the $^{40}Ar/^{39}Ar$ incremental-heating technique (Montanari et al., 1997). Our study resulted in a direct astronomical age control with an unprecedented accuracy and resolution for the interval straddling the Serravallian/Tortonian boundary, thereby extending the existing astronomical timescale in the Mediterranean back to 12.1 Ma. The timescale is based on the continuous deep-marine cyclically bedded succession of Monte Gibliscemi that is tuned to computed time series of past orbital and insolation variations. It provides accurate absolute ages for all biohorizons recorded in the high-resolution calcareous plankton biostratigraphy. Unfortunately, a straightforward comparison with other timescales is hampered by the lack of a magnetostratigraphy. Only calcareous plankton, and then in particular the calcareous nannofossil biochronology is available for this purpose. Ages for calcareous nannofossil events in different (oceanic) basins and according to different timescales are compared with one another in Table 3.

The biochronology obtained from Monte Gibliscemi is particularly relevant for discussing the validity of timescales and the synchroneity of calcareous nannofossil biohorizons. The chronology is consistent with the astrobiochronology independently obtained for the tropical Atlantic (Backman and Raffi, 1997). A diachrony exists for the *D. hamatus* FO, which shows different ages between the Mediterranean and the oceans (tropical Pacific and Atlantic), although this may reflect the rare and discontinuous occurrence of the species in the Monte Gibliscemi section. The occurrence of common *D. kugleri* (FCO and LCO), the *C. miopelagicus* LRO, and even the scattered lowermost occurrences of *C. coalitus* and *D. neohamatus*, have estimated ages that are in good to perfect agreement with the astronomical ages obtained for the same biohorizons in the low-latitude Atlantic (Fig. 6; Table 3). In our opinion, this correspondence cannot be explained other than that these biohorizons are (near-)synchronous between the tropical Atlantic and the Mediterranean and that the astronomical timescales independently es-

Table 3
Comparison of ages for selected calcareous nannofossil events in different (oceanic) basins and according to different time scales

Species	Event	Equatorial Pacific		Event	Ceara Rise	Event	Mediterranean (this paper)
		SCHPS95	CK95				
D. neohamatus	F(C)O	9.56 ± 0.11	–	X	9.771 ± 0.003	FO/X	9.826 ± 0.003
D. hamatus	FO	10.39 ± 0.10	10.390	FO	10.476 ± 0.010	FO	10.150 ± 0.002
C. coalitus	FO	10.71 ± 0.01	10.836	FO	10.794 ± 0.004	FO	10.738 ± 0.001
C. miopelagicus	LO	10.39 ± 0.10	–	LO	10.941 ± 0.010	LRO	10.977 ± 0.002
D. kugleri	LCO	11.34 ± 0.03	11.457	LCO	11.598 ± 0.006	LCO	11.604 ± 0.002
D. kugleri	FCO	11.74 ± 0.04	11.805	FCO	11.877 ± 0.004	FCO	11.889 ± 0.004

Ages for equatorial Pacific events are based on the biostratigraphic data of Raffi et al. (1995) and the time scales of Shackleton et al. (1995; SCHPS95) and Cande and Kent (1995; CK95); ages for equatorial Atlantic (Ceara Rise) events are based on biostratigraphic data of Backman and Raffi (1997) and the astronomical time scale of Shackleton and Crowhurst (1997). The error in the ages is based on the uncertainty in the position of the events. X marks cross-over in abundance (from *D. hamatus* to *D. neohamatus*).

tablished for Ceara Rise (Shackleton and Crowhurst, 1997) and the Mediterranean (this paper) are consistent with one another to within one or two precession cycles. The discrepancies on the order of 10^5 yr with ages obtained for the same events in the eastern equatorial Pacific calibrated to the Cande and Kent (1995) timescale (see also Shackleton and Crowhurst, 1997) may reflect the lower precision of (radio-isotopic) ages assigned to geomagnetic reversal boundaries in CK95, in combination with interpolating spreading rates over millions of years.

7.2. Speculations about the age of reversal boundaries

Despite the lack of a magnetostratigraphy, astronomical ages can be indirectly estimated for the polarity reversals in the studied time interval by exporting the astronomical ages of calcareous nannofossil events from Ceara Rise (and indirectly the Mediterranean) to ODP Leg 138 sites in the eastern equatorial Pacific having a reliable magnetostratigraphy. For this purpose we employed in the first instance the *D. kugleri* FCO and LCO, and the *D. hamatus* FO because these events can be assumed to be near-synchronous between the tropical Atlantic and Pacific (they represent evolutionary changes or a well-defined acme with a relative short duration). Linear interpolation of the sedimentation rate between the indirectly astronomically dated nannofossil datum planes yielded ages for reversal boundaries at ODP Site 845 that are consistently older than the CK95 ages (Age 1 in Table 4). Towards the younger end of Chron C5, the discrepancies are similar to those previously reported from the direct astronomical dating of polarity reversals in younger Miocene sections in the Mediterranean (Hilgen et al., 1995). Note, however, that the additional use of the *C. coalitus* FO results in ages that reveal much larger discrepancies with CK95 at the younger end of Chron C5 while the ages for the older end of Chron C5 become younger than in CK95 (Age 2 in Table 4). At present, we have no explanation for this marked discrepancy. As a consequence, the ages reported in Table 4 should not be considered as definitive. At best they only represent a fair approximation of the true astronomical ages also because the sediment accumulation rate in ODP Leg 138 sites is variable. They should be confirmed and where necessary modified by further studies.

7.3. Serravallian/Tortonian boundary

The evolution of *N. acostaensis* from its immediate ancestor *N. continuosa* was observed by Blow (1969) in a number of tropical localities in Venezuela, Jamaica, Java, and Papua and used to define his N15/N16 zonal boundary. The first occurrence of *N. acostaensis* at these tropical localities, however, resulted from migration (e.g., Zachariasse, 1992). The invasion of *N. acostaensis* at the tropical Ceara Rise has recently been dated at 9.82 Ma using astronomical tuning (Chaisson and Pearson, 1997). This age indeed shows that the FO of *N. acostaensis* in the tropical region is significantly younger than in the Mediterranean. The diachroneity involved is almost

Table 4
Astronomical age estimates for reversal boundaries at ODP Site 845 in the studied time interval and comparison with published ages according to the time scales of Hilgen et al. (1995; HKLLSZ95) and Cande and Kent (1995; CK95)

Event		Position	Range	Age 1	Age 2	HKLLSZ95	CK95
C4Ar.2n	(y)	145.08		9.652 ± 0.047	9.845 ± 0.081	9.629	9.580
C4Ar.2n	(o)	146.70		9.762 ± 0.044	9.929 ± 0.072	9.740	9.642
C5n.1n	(y)	147.86		9.841 ± 0.041	9.989 ± 0.067	–	9.740
C5n.1n	(o)	150.21		10.000 ± 0.035	10.111 ± 0.053	–	9.880
C5n.2n	(y)	150.76		10.037 ± 0.034	10.139 ± 0.051	–	9.920
D. hamatus	**FO**	**157.23**	**157.10–157.35**	**10.476 ± 0.010**	**10.476 ± 0.010**		
C. coalitus	**FO**	**163.38**	**163.15–163.61**	*	**10.794 ± 0.004**		
C5n.2n	(o)	164.93		10.998 ± 0.020	10.914 ± 0.022	–	10.949
C5r.1n	(y)	166.01		11.071 ± 0.020	10.997 ± 0.022	–	11.052
C5r.1n	(o)	166.60		11.111 ± 0.020	11.043 ± 0.022	–	11.099
D. kugleri	**LCO**	**173.78**	**173.56–174.00**	**11.598 ± 0.006**	**11.598 ± 0.006**		
C5r.2n	(y)	174.17		11.613 ± 0.014	11.613 ± 0.014	–	11.476
C5r.2n	(o)	175.77		11.673 ± 0.013	11.673 ± 0.013	–	11.531
D. kugleri	**FCO**	**181.16**	**181.00–181.32**	**11.877 ± 0.004**	**11.877 ± 0.004**		
C5An.1n	(y)	183.73		11.975 ± 0.019	11.975 ± 0.019	–	11.935
C5An.1n	(o)	187.14		12.105 ± 0.030	12.105 ± 0.030	–	12.078

Ages were obtained by exporting astronomical ages of selected calcareous nannofossil events from ODP Site 926 in the equatorial Atlantic to Site 845 in the eastern equatorial Pacific having a reliable magnetostratigraphy, and assuming a low-latitude synchroneity for these events between the Atlantic and Pacific oceans. The ages for the polarity reversals reported in the present table (as Age 1 and Age 2) were calculated on the assumption of a constant sedimentation rate between the astronomically dated calibration points provided by the selected calcareous nannofossil events (indicated in bold). The error in the astronomical age estimate for the reversal boundaries is based on the combined uncertainty in the position of these events at Site 845 (given in Table 3) and in the position and thus age of these events at Site 926. Note that the uncertainty in the position of the polarity reversals has not been incorporated.
(o) indicates older and (y) younger end of (sub)chron. Position of events (at Site 845) are given in metre composite depth (mcd).
* marks unused calibration point.

2 million years for the FO and 0.73 million years if we start from the FRO of *N. acostaensis* in the Mediterranean. In contrast to delayed low-latitude arrival of *N. acostaensis* at Ceara Rise, *P. mayeri* shows a delayed extinction of more than 0.7 million years with respect to the Mediterranean (LO at 10.49 Ma at Ceara Rise, Chaisson and Pearson, 1997; LO at 11.205 Ma in the Mediterranean, this paper). As a result, the N14/N15 and N15/N16 zonal boundaries are strongly diachronous between the low-latitude and the mid- to high-latitude North Atlantic. Ages for the N14/N15 zonal boundary are 10.49 Ma at Ceara Rise and 11.205 Ma in the Mediterranean, whereas ages for the N15/N16 zonal boundary are 9.82 Ma at Ceara Rise and 11.781 or 10.554 Ma in the Mediterranean dependent on whether the FO or FRO of *N. acostaensis* is used to define the N15/N16 zonal boundary.

The Serravallian/Tortonian (S/T) boundary is not yet formally defined but is commonly placed at or close to the *N. acostaensis* FO (Rio et al., 1997) because this bio-event has previously been reported — as the first evolutionary appearance — from the basal part of the Tortonian historical stratotype section of Rio Mazzapiedi–Castellania (Cita and Premoli Silva, 1968), which is assigned to nannofossil zone NN9 on the basis of the presence of the zonal marker *D. hamatus* (Mazzei, 1977). These zonal assignments are conflicting, however, with the common practice to place the N15/N16 boundary at or close to the base of NN8 (see Rio et al., 1997), while our data from Gibliscemi even indicate that the *N. acostaensis* FO actually falls within zone NN7 in the Mediterranean as previously suggested by Foresi et al. (1998). This indicates that the so-called *N. acostaensis* FO at Rio Mazzapiedi–Castellania does not represent the true first occurrence of this species, as recently confirmed by the presence of rare *N. acostaensis* in the top part of the Serravalle Sandstones immediately below the base of the Tortonian stratotype (Miculan, 1997; Foresi et al., 1998). Evidently, the base of the Tortonian stratotype postdates the *N. acostaensis* FO in the Mediterranean.

The base of the Tortonian stratotype is older than the *N. acostaensis* FRO of Foresi et al. (1998). But locating their *N. acostaensis* FRO above the *D. hamatus* FO in the Tortonian stratotype (Foresi et al., 1998) conflicts with our findings at Monte Gibliscemi which indicate that the *D. hamatus*/*bellus* entry is delayed in the Mediterranean and postdates the *N. acostaensis* FRO by several 100,000 years. To solve this discrepancy, we checked the samples of the Tortonian stratotype studied by Foresi et al. (1998). Following our taxonomic criteria (a.o. based on the ratio between typical *N. acostaensis* and small-sized *N. atlantica*), the *N. acostaensis* FRO is positioned lower in the succession, near the base of the Tortonian. Moreover, the dominant right coiling of the neogloboquadrinids indicates that there is no biostratigraphically discernable hiatus at the base of the Tortonian stratotype and that the top part of the underlying Serravalle Sandstone postdates the first influx of the neogloboquadrinids at Monte Gibliscemi in which the coiling direction is essentially random. Our findings further imply that the base of the Tortonian postdates the *P. mayeri* LO and, as a consequence, that all specimens of this species in the Tortonian stratotype should be considered reworked. In conclusion, the Tortonian base in the historical stratotype corresponds almost exactly with the *N. acostaensis* s.s FRO as defined in the present paper and dated at 10.554 Ma. This observation is more or less consistent with Müller (1975) who examined the 'Serravallian part' of the Rio Mazzapiedi–Castellania section and referred it with certainty to NN7, and probably also to NN8 and the lower part of NN9, although the latter could not be confirmed due to the lack of samples from the uppermost part of the Serravalle Sandstone in this section.

We further arrived at an age of 11.8 Ma for the top of the Serravallian stratotype in the Serravalle Scrivia section by linear extrapolation of the sedimentation rate between the *Sphenolithus heteromorphus* LO (13.5 Ma, Rio et al., 1997) and the *Calcidiscus premacintyrei* (12.3 Ma, Rio et al., 1997). This admittedly rough age estimate indicates that there is gap between the top of the Serravallian stratotype and the base of the Tortonian stratotype as previously suggested by Rio et al. (1997) among others. These observations potentially render all bio-events in the interval between 11.8 and 10.554 Ma suitable for delimiting the S/T boundary. Despite the tectonic deformation and lack of a magnetostratigraphy, section Gibliscemi remains a potential candidate for defining the Tortonian GSSP because it contains a continuous and astronomically dated succession over this interval with an outstanding calcareous plankton biostratigraphy and biochronology, and intercalated ash layers. The alternative section of Monte dei Corvi has as yet not been astronomically dated but is similarly unsuitable for establishing a reliable magnetostratigraphy (Montanari et al., 1997). A potentially serious shortcoming is that neither the *D. kugleri* acme nor the first influx of the neogloboquadrinids have been reported from Monte dei Corvi. The lack of these bio-events may indicate the presence of a hiatus in this section in the critical interval straddling the boundary.

Acknowledgements

C.G. Langereis, S. Iaccarino, L.J. Lourens, A.A.M. van Hoof and A. Santarelli are thanked for their help in the field, G. Ittmann and G.J. van 't Veld for washing the micropaleontological samples, W. Wei and an anonymous referee for reviewing the manuscript and L.J. Lourens and S. Iaccarino for discussion. This study was partly supported by the Netherlands Geosciences Foundation (GOA) with financial aid from the Netherlands Organisation of Scientific Research (NWO).

Appendix A. Taxonomic appendix of plankton foraminifera

The list includes all the taxa cited in the paper. The taxonomic concepts are those of Kennett and Srinivasan (1983), Bolli and Saunders (1985), Iaccarino (1985), Hemleben et al. (1989) and those discussed in the paper.

Globigerinoides subquadratus Brönnimann = *Globigerinoides subquadrata* Brönnimann, 1954; Kennett and Srinivasan, 1983, pl. 16, figs. 1–3.

Globoquadrina sp. 1 (this paper, Plate 1, 1–7).

Globorotalia partimlabiata Ruggieri and Sprovieri = *Globorotalia acrostoma partimlabiata* Ruggieri and Sprovieri, 1970, text-fig. 3; Giannelli and Salvatorini, 1976, fig. 1, nos. 1–2; (this paper, Plate 4, 4–6).

Globorotaloides falconarae Giannelli and Salvatorini = *Globorotaloides falconarae* Giannelli and Salvatorini, 1976, pl. 2, figs. 1–6; (this paper, Plate 1, 8–12).

Neogloboquadrina acostaensis (Blow) = *Globorotalia acostaensis* Blow, 1959, pl. 17, figs. 106a–c; (this paper, Plate 2, 10–12).

Neogloboquadrina atlantica (Berggren) = *Globigerina atlantica* Berggren, 1972, pl. 1, figs. 1–7; Poore and Berggren, 1975, pls. 1–3; Poore, 1979, pl. 16, figs. 1–12; (this paper, Plate 2, 1–7).

Neogloboquadrina 4-chambered type (this paper, Plate 2, 8 and 9).

Paragloborotalia mayeri (Cushman and Ellisor) = *Globorotalia mayeri* Cushman and Ellisor, 1939, pl. 2, figs. 4a–c; Bolli and Saunders, 1985, fig. 26, nos. 31–43; (this paper, Plate 4, 1–3).

Appendix B. Taxonomic appendix of calcareous nannofossils

The list includes all the taxa cited in the paper. The taxonomy and relative biostratigraphical references are those of Perch-Nielsen (1985), Young and Brown (1997) and those discussed in the paper.

Catinaster Martini and Bramlette, 1963
C. coalitus Martini and Bramlette, 1963 (this paper, Plate 5, 10–12)
Coccolithus Schwarz, 1894 *C. miopelagicus* Bukry, 1971 (this paper, Plate 5, 6 and 7)
Discoaster Tan, 1927
D. bellus Bukry and Percival, 1971 (this paper, Plate 5, 15)
D. bolli Martini and Bramlette, 1963
D. brouweri (Tan, 1927) Bramlette and Riedel, 1954
D. exilis Martini and Bramlette, 1963
D. hamatus Martini and Bramlette, 1963 (this paper, Plate 5, 17–19)
D. intercalaris Bukry, 1971
D. kugleri Martini and Bramlette, 1963 (this paper, Plate 5, 20)
D. micros Theodoridis, 1984 (this paper, Plate 5, 8)
D. neohamatus Bukry and Bramlette, 1969 (this paper, Plate 5, 20)
D. variabilis Martini and Bramlette, 1963
Helicosphaera Kamptner, 1954
H. stalis Theodoridis, 1984
H. walbersdorfensis Muller, 1974

References

Backman, J., Raffi, I., 1997. Calibration of Miocene nannofossil events to orbitally-tuned cyclostratigraphies from Ceara Rise. Proc. ODP., Sci. Res. 154, 83–99.

Backman, J., Shackleton, N.J., 1983. Quantitative biochronology of Pliocene and early Pleistocene calcareous nannofossils from Atlantic, Indian and Pacific Oceans. Mar. Micropaleontol. 8, 141–170.

Berggren, W.A., Kent, D.V., Swisher, C.C., Aubry, M.-P., 1995. A revised Cenozoic geochronology and chronostratigraphy. Soc. Econ. Paleontol. Mineral. Spec. Publ. 54, 129–212.

Blow, W.H., 1959. Age, correlation and biostratigraphy of the upper Tocuyo (San Lorenzo) and Pozon Formations, eastern Falcón, Venezuela. Bull. Am. Paleontol. 39, 67–251.

Blow, W.H., 1969. Late Middle Eocene to Recent planktonic foraminiferal biostratigraphy. Proc. Int. Conf. Planktonic Microfossils, Geneva, 1967, 1, pp. 199–442.

Bolli, H.M., 1957. Planktonic foraminifera from the Oligocene–Miocene Cipero and Lengua Formations of Trinidad, B.W.I. U.S. Natl. Mus. Bull. 215, 97–123.

Bolli, H.M., Saunders, J.B., 1985. Oligocene to Holocene low latitude planktonic Foraminifera. In: Bolli, H.M., Saunders, J.B., Perch-Nielsen, K. (Eds.), Plankton Stratigraphy. Cambridge Univ. Press, Cambridge, pp. 155–262.

Bukry, D., 1973. Low latitude coccolith biostratigraphic zonation. Init. Rep. DSDP 15, 685–703.

Bukry, D., 1978. Biostratigraphy of Cenozoic marine sediments by calcareous nannofossils. Micropaleontology 24, 44–60.

Cande, S.C., Kent, D.V., 1995. Revised calibration of the Geomagnetic Polarity Time Scale for the Late Cretaceous and Cenozoic. J. Geophys. Res. 100, 6093–6095.

Chaisson, W.P., Pearson, P.N., 1997. Planktonic foraminifer biostratigraphy at Site 925: Middle Miocene–Pleistocene. Proc. ODP, Sci. Results 154, 3–31.

Chamley, H., Meulenkamp, J.E., Zachariasse, W.J., van der Zwaan, G.J., 1986. Middle to Late Miocene marine ecostratigraphy: clay minerals, planktonic foraminifera and stable isotopes from Sicily. Oceanol. Acta 9, 227–238.

Chepstow-Lusty, A., Backman, J., Shackleton, N.J., 1989. Comparison of Upper Pliocene *Discoaster* abundance variations from North Atlantic Sites 552, 607, 658, 659 and 662: further evidence for marine plankton responding to orbital forcing. Proc. ODP, Sci. Results 108, 121–141.

Chepstow-Lusty, A., Shackleton, N.J., Backman, J., 1992. Upper Pliocene *Discoaster* abundance variations from the Atlantic, Pacific and Indian Oceans: the significance of productivity pressure at low latitudes. Mem. Sci. Geol. Univ. Padova 44, 357–373.

Cita, M.B., Premoli Silva, I., 1968. Evolution of the planktonic foraminiferal assemblages in the stratigraphic interval between the type Langhian and the type Tortonian and the biozonation of the Miocene of Piedmont. G. Geol. 35, 1051–1081.

Coccioni, R., Galeotti, S., Di Leo, R., 1994. The first occurrence of *Neogloboquadrina atlantica* (Berggren) in the Mediterranean. G. Geol. 56, 127–138.

de Visser, J.P., 1991. Clay mineral stratigraphy of Miocene to Recent marine sediments in the central Mediterranean. Geol. Ultraiectina 75, 243 pp.

Dowsett, H.J., Ishman, S.E., 1995. Middle Pliocene planktonic and benthic foraminifers from the subarctic North Pacific: Sites 883 and 887. Proc. ODP, Sci. Results 145, 141–156.

Foresi, L.M., Iaccarino, S., Mazzei, R., Salvatorini, G., 1998. New data on Middle to Late Miocene calcareous plankton

biostratigraphy in the Mediterranean area. Riv. Ital. Paleontol. Stratigr. 104, 95–114.

Fornaciari, E., Di Stefano, A., Rio, D., Negri, A., 1996. Middle Miocene quantitative calcareous nannofossil biostratigraphy in the Mediterranean region. Micropaleontology 42, 37–63.

Gartner, S., 1992. Miocene nannofossil chronology in the North Atlantic, DSDP Site 608. Mar. Micropaleontol. 18, 307–331.

Giannelli, L., Salvatorini, G., 1976. Due nuove specie di foraminiferi planctonici del Miocene. Boll. Soc. Paleontol. Ital. 15, 167–173.

Hemleben, C., Spindler, M., Anderson, O.R., 1989. Modern Planktonic Foraminifera. Springer, New York, 363 pp.

Hilgen, F.J., 1987. Sedimentary cycles and high-resolution chronostratigraphic correlations in the Mediterranean. Newsl. Stratigr. 17, 109–127.

Hilgen, F.J., 1991. Astronomical calibration of Gauss to Matuyama sapropels in the Mediterranean and implication for the Geomagnetic Polarity Time Scale. Earth Planet. Sci. Lett. 104, 226–244.

Hilgen, F.J., Krijgsman, W., Langereis, C.G., Lourens, L.J., Santarelli, A., Zachariasse, W.J., 1995. Extending the astronomical (polarity) time scale into the Miocene. Earth Planet. Sci. Lett. 136, 495–510.

Huddlestun, P.F., 1984. Planktonic foraminiferal biostratigraphy, Deep Sea Drilling Project Leg 81. Init. Rep. DSDP 81, 429–438.

Iaccarino, S., 1985. Mediterranean Miocene and Pliocene planktic foraminifera. In: Bolli, H.M., Saunders, J.B., Perch-Nielsen, K. (Eds.), Plankton Stratigraphy. Cambridge Univ. Press, pp. 283–314.

Kennett, J.P., Srinivasan, M.S., 1983. Neogene Planktonic Foraminifera: A Phylogenetic Atlas. Hutchinson and Ross, Stroudsburg, PA, 265 pp.

Krijgsman, W., Hilgen, F.J., Langereis, C.G., Santarelli, A., Zachariasse, W.J., 1995. Late Miocene magnetostratigraphy, biostratigraphy and cyclostratigraphy from the Mediterranean. Earth Planet. Sci. Lett. 136, 475–494.

Langereis, C.G., van Hoof, A.A.M., Hilgen, F.J., 1994. Steadying the rates. Nature 369, 615.

Laskar, J., 1990. The chaotic motion of the solar system: a numerical estimate of the size of the chaotic zones. Icarus 88, 266–291.

Laskar, J., Joutel, F., Boudin, F., 1993. Orbital, precessional, and insolation quantities for the Earth from −20 Myr to +10 Myr. Astron. Astrophys. 270, 522–533.

Lourens, L.J., Hilgen, F.J., Zachariasse, W.J., van Hoof, A.A.M., Antonarakou, A., Vergnaud-Grazzini, C., 1996. Evaluation of the Plio-Pleistocene astronomical time scale. Paleoceanography 11, 391–413.

Mazzei, R., 1977. Biostratigraphy of the Rio Mazzapiedi–Castellania section (type-section of the Tortonian) based on calcareous nannoplankton. Atti Soc. Toscana Sci. Nat., Mem. A 84, 15–24.

Miculan, P., 1997. Planktonic foraminiferal biostratigraphy of the Tortonian historical stratotype, Rio Mazzapiedi–Catellania section, northwestern Italy. In: Montanari, A., Odin, G.S., Coccioni, R. (Eds.), Miocene Stratigraphy: An Integrated Approach. Developments in Palaeontology and Stratigraphy, 15. Elsevier, Amsterdam, pp. 97–106.

Montanari, A., Beaudoin, B., Chan, L.S., Coccioni, R., Deino, A., De Paolo, D.J., Emmanuel, L., Fornaciari, E., Kruge, M., Lundblad, S., Mozzato, C., Portier, E., Renard, M., Rio, D., Sandroni, P., Stankiewicz, A., 1997. Integrated stratigraphy of the Middle and Upper Miocene pelagic sequence of the Cònero Riviera (Marche region, Italy). In: Montanari, A., Odin, G.S., Coccioni, R. (Eds.), Miocene Stratigraphy: An Integrated Approach. Developments in Palaeontology and Stratigraphy, 15. Elsevier, Amsterdam, pp. 409–450.

Müller, C., 1975. Calcareous nannoplankton from the type Serravallian. Proc. Regional Committee on Mediterranean Neogene Stratigraphy, Bratislava, pp. 49–52.

Olafsson, G., 1991. Quantitative calcareous nannofossil biostratigraphy and biochronology of early through late Miocene sediments from DSDP Hole 608. Medd. Stockholms Univ. Inst. Geol. Geok., 203.

Perch-Nielsen, K., 1985. Cenozoic calcareous nannofossils. In: Bolli, H.M., Saunders, J.B., Perch-Nielsen, K. (Eds.), Plankton Stratigraphy. Cambridge Univ. Press, Cambridge, pp. 427–554.

Poore, R.Z., 1979. Oligocene through Quaternary planktonic foraminiferal biostratigraphy of the North Atlantic: DSDP Leg 49. Init. Rep. DSDP 49, 447–517.

Postma, G., Hilgen, F.J., Zachariasse, W.J., 1993. Precession-punctuated growth of a late Miocene submarine-fan lobe on Gavdos (Greece). Terra Nova 5, 438–444.

Raffi, I., Flores, J.-A., 1995. Pleistocene through Miocene calcareous nannofossils from eastern equatorial Pacific Ocean (Leg 138). Proc. ODP, Sci. Results 138, 233–281.

Raffi, I., Rio, D., d'Atri, A., Fornaciari, E., Rocchetti, S., 1995. Quantitative distribution patterns and biomagnetostratigraphy of Middle to Late Miocene calcareous nannofossils from equatorial Indian and Pacific Oceans (Legs 115, 130, and 138). Proc. ODP, Sci. Results 138, 479–502.

Raffi, I., Backman, J., Rio, D., 1998. Evolutionary trends of tropical calcareous nannofossils in the late Neogene. Mar. Micropaleontol. 35, 17–41.

Remane, J., Bassett, M.G., Cowie, J.W., Gohrbrandt, K.H., Richard Lane, H., Michelsen, O., Naiwen, W., 1996. Revised guidelines for the establishment of global chronostratigraphic standards by the International Commission on Stratigraphy (ICS). Episodes 19, 77–81.

Rio, D., Fornaciari, E., Raffi, I., 1990a. Late Oligocene through early Pleistocene calcareous nannofossils from western equatorial Indian Ocean (Leg 115). Proc. ODP, Sci. Results 115, 175–221.

Rio, D., Raffi, I., Villa, G., 1990b. Pliocene–Pleistocene calcareous nannofossil distribution patterns in the western Mediterranean. Proc. ODP, Sci. Results 107, 513–533.

Rio, D., Cita, M.B., Iaccarino, S., Gelati, R., Gnaccolini, M., 1997. Langhian, Serravallian, and Tortonian historical stratotypes. In: Montanari, A., Odin, G.S., Coccioni, R. (Eds.), Miocene Stratigraphy: An Integrated Approach. Developments in Palaeontology and Stratigraphy, 15. Elsevier, Amsterdam, pp. 57–87.

Schenau, S.J., Antonarakou, A., Hilgen, F.J., Lourens, L.J., Nijenhuis, I.A., van der Weijden, C.H., Zachariasse, W.J., 1999. Organic-rich layers in the Metochia section (Gavdos, Greece): evidence for a single mechanism of sapropel formation during the past 10 My. Mar. Geol. 153, 117–135.

Shackleton, N.J., Crowhurst, S., 1997. Sediment fluxes based on an orbitally tuned time scale 5 Ma to 14 Ma, Site 926. Proc. ODP, Sci. Results 154, 69–82.

Shackleton, N.J., Crowhurst, S., Hagelberg, T., Pisias, N.G., Schneider, D.A., 1995. A new late Neogene timescale: application to leg 138 sites. Proc. ODP, Sci. Results 138, 73–101.

Sprovieri, R., di Stefano, E., Becquey, S., Bonomo, S., Caravà, N., 1996. Calcareous plankton biostratigraphy and cyclostratigraphy at the Serravallian–Tortonian boundary. Palaeopelagos 6, 437–453.

Theodoridis, S., 1984. Calcareous nannofossil biozonation of the Miocene and revision of the Helicoliths and Discoasters. Utrecht Micropaleontol. Bull. 32, 272 pp.

Tjalsma, R.C., 1971. Stratigraphy and foraminifera of the Neogene of the Eastern Guadalquivir basin, S. Spain. Utrecht Micropaleontol. Bull. 4, 109 pp.

Young, J.R., Brown, P.R., 1997. Cenozoic calcareous nannoplankton classification. J. Nannoplankton Res. 19, 36–47.

Zachariasse, W.J., 1975. Planktonic foraminiferal biostratigraphy of the late Neogene of Crete (Greece). Utrecht Micropaleontol. Bull. 11, 171 pp.

Zachariasse, W.J., 1992. Neogene planktonic foraminifers from Sites 761 and 762 off Northwest Australia. Proc. ODP, Sci. Results 122, 665–675.

Zachariasse, W.J., Aubry, M.-P., 1994. Origin and early dispersal of Neogloboquadrina. Paleobios 16 (2), 68.

Zachariasse, W.J., Spaak, P., 1983. Middle Miocene to Pliocene paleoenvironmental reconstruction of the Mediterranean and adjacent Atlantic Ocean: planktonic foraminiferal record of southern Italy. Utrecht Micropaleontol. Bull. 30, 91–110.